Received: 20 April 2019 | Revised: 16 September 2019 | Accepted: 21 September 2019

DOI: 10.1111/bre.12413

ORIGINAL ARTICLE

Basin Research IAS EAGE WILEY

The changing Patagonian landscape: Erosion and westward sediment transfer paths in northern Patagonia during the Middle and Late Pleistocene

Tania Villaseñor[1,2] | **Daniel Tentori**[3] | **Kathleen M. Marsaglia**[4] | **Luisa Pinto**[1,5]

[1]Departamento de Geología, Universidad de Chile, Santiago, Chile

[2]Núcleo Milenio Paleoclima, Santiago, Chile

[3]Dipartimento di Scienze della Terra, Sapienza Università di Roma, Roma, Italia

[4]Department of Geological Sciences, California State University Northridge, Northridge, CA, USA

[5]Escuela de Ingeniería y Ciencias, Facultad de Ciencias Físicas y Matemáticas, Universidad de Chile, Santiago, Chile

Correspondence
Tania Villaseñor, Instituto de Ciencias de la Ingeniería, Universidad de O'Higgins, Rancagua, Chile.
Email: tania.villasenor@uoh.cl

Funding information
Fondo Nacional de Desarrollo Científico y Tecnológico, Grant/Award Number: 3170611

Abstract

Pleistocene glaciations have promoted important landscape transformations as a result of high rates of erosion and rapid sediment evacuation to adjacent marine basins. In the Patagonian Andes the role of the Patagonian Ice Sheet on landscape evolution, in particular the spatial patterns of glacial erosion and its influence on sediment fluxes, is poorly documented. Here, we investigate the Middle and Late Pleistocene sedimentary record of the continental slope from Ocean Drilling Program (ODP) Site 861, offshore Patagonia (46°S), to evaluate the link between glaciations, mountain range erosion and continental margin strata formation. Petrographic analysis of the sand-size fraction (0.063–2 mm) and εNd and $^{87}Sr/^{86}Sr$ measurements in the silt-size fraction (10–63 μm) indicate that glacial erosion over the last 350,000 years has focused within the Patagonian Batholith, with a minor influence of a proximal source to the drilling site, the Chonos Metamorphic Complex. This shows that erosion has focused in the core of the northern Patagonian Andes, coinciding roughly with the location of the Liquiñe-Ofqui Fault Zone and the zone of concentrated precipitation during glaciations, suggesting a combined climatic and structural control on glacial erosion. Temporal variation in the provenance signal is contemporaneous with a marked change in the stratigraphy of ODP Site 861 that occurred after the glaciation of MIS 8 (~240 kyr ago). Before MIS 8, a restricted provenance signal and coarse lithofacies accumulated on the continental slope indicates spatially restricted erosion and efficient transfer of sediment towards the ocean. In contrast, very high provenance variability and finer continental slope lithofacies accumulation after MIS 8 suggest a disorganized expansion of the areas under erosion and a more distal influence of ice sediment discharge to this site. We argue that this change may have been related to a re-organization of the drainage patterns of the Patagonian Ice Sheet and flow of outlet glaciers to the continental margin during the last two glaciations.

KEYWORDS

glacial erosion, Ocean Drilling Program, Patagonia, Patagonian Ice Sheet, sediment provenance, source to sink

1 | INTRODUCTION

Constraining the relative influence of climate and tectonics on continental erosion is crucial to understand the formation and destruction of mountain ranges and the dynamics of sedimentary basins. There is evidence that Pleistocene glaciations enhanced orogen erosional processes on a global scale (Herman et al., 2013) and promoted increased landscape relief, especially in mid-latitude regions (40–60°) by the cyclic advance and retreat of temperate glaciers (Champagnac, Valla, & Herman, 2014). Even though the relation between climate and tectonics on mountain building is complex (e.g., Champagnac, Molnar, Sue, & Herman, 2012), glacial erosion appears to be relevant to mountain range topography, erosion and sediment evacuation (Egholm, Nielsen, Pedersen, & Lesemann, 2009; Gulick et al., 2015; Herman et al., 2013; Molnar & England, 1990; Montgomery, Balco, & Willett, 2001; Yanites & Ehlers, 2012). Glacially-influenced landscapes in mid-latitudes represent a prime location for the study of patterns of erosion and the mode of sediment transfer from source to sink given the sensitivity of temperate glaciers to climate changes, as well as their erosional power and thus capacity for shaping the landscape. In such landscapes, repeated glaciations during the Pleistocene have led to considerable temporal and spatial variability in the processes of glacial erosion and glacigenic sediment delivery to adjacent marine basins (Cofaigh et al., 2012; Montelli, Dowdeswell, Ottesen, & Johansen, 2017; VanLaningham, Pisias, Duncan, & Clift, 2009; Villaseñor, Jaeger, & Foster, 2016). Mid-latitude marine sedimentary records from active continental margins are therefore particularly suited to reconstruct processes of glacial erosion of orogens and sediment evacuation spanning multiple glacial cycles and across large regions.

The latitudinal variation in climatic and tectonic regimes of the Patagonian Andes (Figure 1) makes it a relevant location to study processes of glacial erosion and sediment fluxes to the Pacific Ocean. This subduction-related mountain belt spans a large latitudinal range that intersects the Westerlies Wind Belt (WWB), concentrating precipitation on

Highlights

- Petrographic and Sr and Nd isotopic studies of marine sand and silt fractions from core samples recovered at Ocean Drilling Program Site 861.
- Sediment provenance results provide insights into patterns of erosion of the northern Patagonian Andes during the Middle-Late Pleistocene.
- Temporal variation in provenance signal and marine stratigraphy suggest re-organization of ice drainage patterns and sediment dispersal along the South American continental margin around 240 kyr ago.

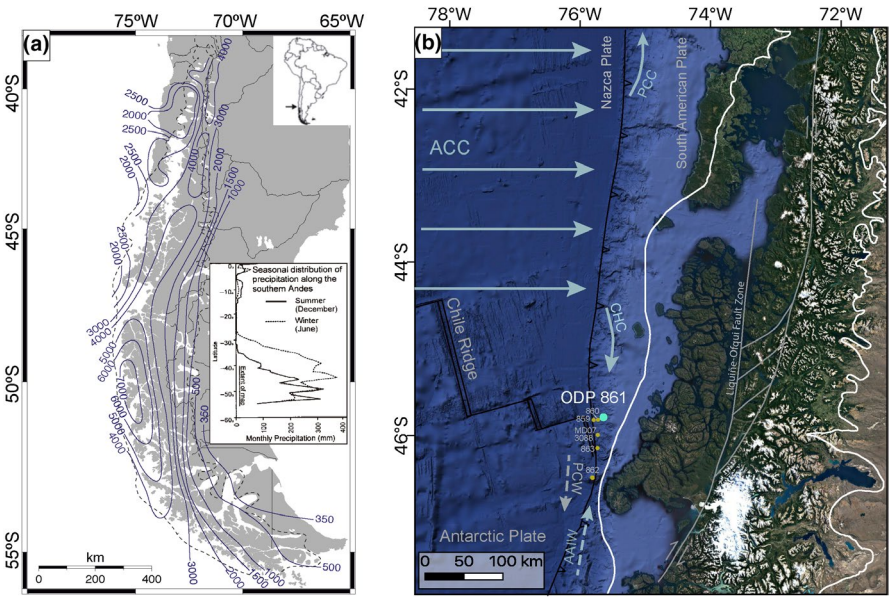

FIGURE 1 (a) Western border of South America showing the modern average precipitation pattern in Patagonia, and an inset box showing latitudinal variation of the distribution of precipitation. Modified from Montade et al. (2013). (b) Landcover image of northern Patagonia (Chile) and morphological features of the region. The location of ODP Site 861 is in green, and other drilling sites mentioned in the text are presented with yellow symbols. White solid line represents the extent of PIS during the LGM; note that the western extent between 43 and 47°S is speculated (see text). Modern oceanic circulation of the study area is included. AAIW, Antarctic Intermediate Water; ACC, Antarctic Circumpolar Current; CHC, Cape Horn Current; PCC, Peru-Chile Current; PCW, Pacific Central Water. The Liquiñe-Ofqui Fault Zone is delineated in grey

the windward side of the orogen and favouring the formation of the Patagonian Ice Sheet (PIS) during the Pleistocene (Rabassa, Coronato, & Martinez, 2011). The PIS is considered the dominant agent of landscape evolution in the region (Montgomery et al., 2001; Ramos & Ghiglione, 2008; Thomson, 2002; Thomson et al., 2010). A recent modelling study identified an erosion hotspot in northern Patagonia between 42 and 46°S around 2 Ma that resulted from the northward migration of the WWB during Pleistocene glaciations (Herman & Brandon, 2015).

The fate of the glacigenic sediment at these latitudes is poorly understood. Previous provenance analyses of marine sediment from sites of Ocean Drilling Program (ODP) Leg 141 provide insights into offshore sedimentation processes. This expedition drilled five sites offshore Patagonia (site ODP 859, 860, 861, 862, 863; Figure 1b) that extracted a Plio-Pleistocene sequence dominated by silty clays and clayey silts with intercalations of silt, sand and gravel layers that grade downward into equivalent lithified sequences (Behrmann et al., 1992). The sand composition of samples from all sites of this expedition shows that sediment accumulated due to extensive onshore erosion of basement rocks (Heberer, Behrmann, & Rahn, 2011; Heberer, Roser, Behrmann, Rahn, & Kopf, 2010; Marsaglia, Torrez, Padilla, & Rimkus, 1995). Kilian and Behrmann (2003) use Sr and Nd isotopes in bulk sediment samples from these same sites to determine variations in sediment provenance and link it to Plio-Pleistocene glaciations. Siani et al. (2010) analysed the clay mineralogy of sediment from ocean drilling site MD07-3088 (Figure 1b) and related it to rapid variations in ice extent since 22 kyr BP. However, marine sediment provenance signals in this region are complex since they reflect fluctuations of glacial erosion patterns, ice flow paths, and marine sediment transfer and dispersal, which are modulated by climate, oceanic circulation and sea level. Understanding of these processes is a primary goal in the study of sediment-routing systems (Jaeger & Koppes, 2016), which remain incompletely understood in northern Patagonia (e.g., Strand, Marsaglia, & Forsythe, 1995; Thornburg & Kulm, 1987; Völker, Geersen, Contreras-Reyes, & Reichert, 2013).

In this investigation we evaluate the link between Middle to Late Pleistocene glaciations and mountain range erosion in northern Patagonia by conducting a provenance analysis of the siliciclastic sediment that accumulated on the continental slope during this period of time. We evaluate the likely sources of sand (0.063–2 mm) and silt (10–63 μm) fractions from cores recovered on ODP Leg 141 at Site 861 offshore northern Patagonia (Figure 1b) and use these data to reconstruct erosion patterns of the Patagonian Andes and sediment transfer paths to the continental slope. Longitudinal variations in the bedrock geology and its isotopic signature (Pankhurst, Weaver, Hervé, & Larrondo, 1999) in northern Patagonia (Figure 2) provide favourable conditions to reconstruct sediment provenance using mineral composition of the sand-size fraction, and Sr and Nd isotopic analysis of the silt-size fraction. This allows distinguishing the areas of the Patagonian Andes undergoing erosion and tracing the paths by which that material is transferred to the continental margin. Comparison of the sediment provenance signals with the stratigraphy of the Middle to Late Pleistocene continental slope sedimentary sequence provides a first approximation of the processes of glacial erosion and glacimarine sediment accumulation at the glacial–interglacial timescales in northern Patagonia.

2 | REGIONAL SETTING

2.1 | Patagonian Andes

The orogeny of the Patagonian Andes is the result of subduction of the Nazca and Antarctic plates under the South

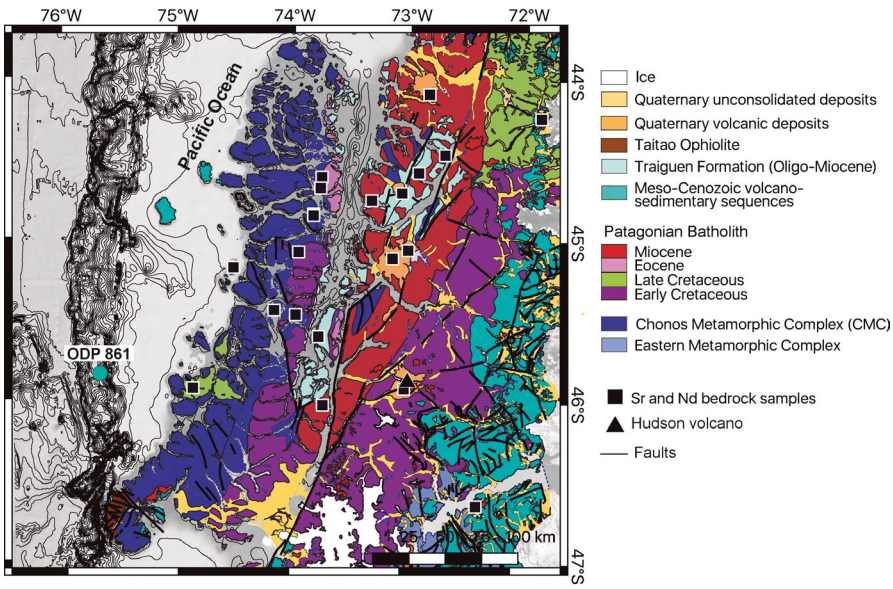

FIGURE 2 Geology of northern Patagonia. Black squares show the location of bedrock samples with Sr and Nd isotopic data used to analyse marine sediment provenance. The bathymetric intervals are every 100 m. Geological information from Pankhurst et al. (1999), Sernageomin (2003), and Encinas et al. (2016). To see this figure in colours, please consult the online version of this manuscript

American plate during the Cenozoic (Pardo-Casas & Molnar, 1987; Ramos & Ghiglione, 2008; Thomson, Hervé, & Stöckhert, 2001). The two subducting plates are separated by the actively spreading Chile Ridge, forming a triple junction at the trench, currently located at 46.3°S, about 50 km southwest of ODP Site 861 (Figure 1b). Subduction of the Chile Ridge beneath the South American plate began at 54–55°S around 14–15 Ma and progressively migrated northward until reaching its current position (Cande & Leslie, 1986; Thomson et al., 2001; Figure 1b). Most deformation of the Patagonian Andes predates ridge subduction, especially in the study area, where ridge subduction has likely had minimal influence on denudation of the upper plate (Blisniuk et al., 2006; Heberer et al., 2011; Thomson et al., 2001). A significant part of the inboard crustal deformation in the study area is accommodated along the Liquiñe-Ofqui Fault Zone (LOFZ), a major intra-arc dextral transpressional fault system of the Patagonian Andes (Cembrano et al., 2002). The LOFZ is seismically active (Lange et al., 2008) and has been associated with volcanic activity, basement uplift, and exhumation initiated between 16 and 10 Ma (Cembrano et al., 2002; Thomson, 2002).

The west flank of the Northern Patagonian Andes comprises two main margin-parallel belts, from west to east: the Chonos Metamorphic Complex (CMC) and the Patagonian Batholith (Figure 2). The CMC is of Late Triassic age and has been interpreted as a subduction complex (Hervé, Fanning, & Pankhurst, 2003) composed of low-grade metasedimentary rocks, namely metasandstone, chert, metapelite and greenschist. This unit has been divided in an Eastern belt, with rocks that are metamorphosed to pumpellyite–actinolite facies, and a Western belt characterized by a transition between greenschist and albite–epidote–amphibolite facies (Hervé, Mpodozis, Davidson, & Godoy, 1981; Willner, Hervé, & Massonne, 2000). The Patagonian Batholith forms most of the Patagonian Andes, occupying the range axis. This batholith is of Late Jurassic to Late Cenozoic age and consists mostly of hornblende-biotite granodiorite and tonalite (Pankhurst et al., 1999). It comprises five age zones, from west to east: Late Cretaceous, Early Cretaceous, Eocene, early Miocene, and Early to Late Cretaceous (Figure 2). Each of these zones presents characteristic signatures in Sr and Nd isotopic compositions, with overall values that are distinct from metamorphic rocks of the CMC (Pankhurst et al., 1999). The Traiguen Formation comprises a small longitudinal band between CMC and the Patagonian Batholith, composed of volcano-sedimentary rocks of Oligocene-early Miocene age (Encinas et al., 2016). The easternmost part of the study area comprises Meso-Cenozoic volcano-sedimentary rocks (Figure 2) that are remnants of the volcanism associated to the intrusions that formed the North Patagonian Batholith and deformation of the Patagonian foreland (Suárez, Cruz, & Bell, 2000). Several Quaternary volcanoes located in the study area, including the Hudson volcano - the most active in the region (Carel, Siani, & Delpech, 2011; Naranjo & Stern, 1998) - have produced volcanic deposits composed of lavas and pyroclasts of basaltic to dacitic composition (D'Orazio et al., 2003; Figure 2).

2.2 | Glaciations in Patagonia

Increased tectonic uplift of the Patagonia Andes driven by a period of rapid increase in convergence rates between 28 and 26 Ma triggered orographically enhanced precipitation on the windward (western) flank, leading to increased erosion rates by fluvial incision (Thomson et al., 2001). Further climate cooling during the Cenozoic promoted the formation of glaciers in Patagonia around 6–7 Ma (Mercer & Sutter, 1982), with evidence of glacial incision on the western margin of Patagonia (Christeleit, Brandon, & Shuster, 2017) coeval with the acceleration of erosion rates in the region around 5–7 Ma (Thomson et al., 2010).

The Patagonian Andes at the latitude of the study area have modern annual mean precipitation in the 5,000–10,000 mm range with small seasonal variation, producing very humid conditions on the west side of the orogen, which sustains the temperate glaciers in the region (Figure 1a). Precipitation patterns in Patagonia are controlled by the intensity and location of the WWB that shifts seasonally between 50°S in winter when it expands, and 55°S in summer when it contracts (Figure 1a; Garreaud, Lopez, Minvielle, & Rojas, 2013). Similar latitudinal variations of the WWB have occurred during past glaciations in which its core migrated around 10° in latitude, with a more equatorward position (~42°S) under glacial conditions, and a more poleward position (~52°S) during interglacials (e.g., Lamy et al., 2010), leading to increased precipitation in northern Patagonia during glaciations (Lamy, Hebbeln, & Wefer, 1999; Moreno & León, 2003). This favoured the formation of the PIS that covered the Patagonian Andes between 37 and 56°S during the Pleistocene (Rabassa et al., 2011; Figure 1b). The extension of the PIS during past glaciations is relatively well-constrained on its eastern flank based on the analysis of moraine deposits which chronologies appear in phase with northern hemisphere glaciations (Hein et al., 2017; Kaplan, Douglass, Singer, Ackert, & Caffee, 2005; Singer, Ackert, & Guillou, 2004). However, the extension of the PIS on its western side is poorly constrained (Glasser & Ghiglione, 2009; Glasser, Jansson, Harrison, & Kleman, 2008) and modelling results have not been tested against field data (Hubbard, Hein, Kaplan, Hulton, & Glasser, 2005; Hulton, Purves, McCulloch, Sugden, & Bentley, 2002). Glacial deposits in the western flank of the PIS have been found submerged under the Pacific Ocean and presumed as formed during the last glaciation (DaSilva, Anderson, & Stravers, 1997). The maximum areal extent

of the PIS, known as the Greatest Patagonian Glaciation (GPG), developed ~1 Ma (Rabassa et al., 2011); glaciations that followed have been less extensive (Kaplan, Hein, Hubbard, & Lax, 2009).

2.3 | Sediment dispersal in Northern Patagonia fjords and continental margin

Present glacial configuration in northern Patagonia comprises alpine glaciers as well as tidewater glaciers that radiate from the Northern Patagonia Ice Sheet and deliver sediment to a system of fjords that trap most of this sediment (Fernandez et al., 2016). The morphology of the coast of northern Patagonia, characterized by deep fjords and the Chonos Archipelago, inhibits the direct fluvial transport of clastic sediments derived from the Patagonian Andes to the continental margin during interglacials (Völker et al., 2013). Ice-sheet growth enhanced erosion rates and sediment transport capacity, which resulted in the delivery of relatively large amounts of terrigenous debris to the continental margin (Strand et al., 1995; Völker et al., 2013).

Modern water circulation in the fjords consists of a surface estuarine water mass (Chilean Fjord Water) flowing out of the fjords between 0 and 30 m depth, and more saline water masses flowing in the opposite direction between 30 and 150 m depth (Antarctic Intermediate Water) and 150 m to the bottom (Equatorial Subsurface Water; Sievers & Silva, 2008; Silva & Guzman, 2006). The complex geography of fjords and channels constrain the circulation of water, with limited number of narrow exit paths across the fjords (Sievers & Silva, 2008). The modern sedimentary infill of the fjords comprises ice-proximal to ice-distal glacimarine to non-glacial (modern) facies (DaSilva et al., 1997) that is formed by shifting hydrodynamic conditions as glaciers retreated in response to changes in precipitation patterns during the last glacial cycle (Bertrand, Hughen, Sepúlveda, & Pantoja, 2012, 2014). Seismic facies analyses from the Patagonia fjords region indicate that the sedimentary record is obliterated during ice advance owing to sediment excavation and reworking (DaSilva et al., 1997).

In northern Patagonia, oceanic surface circulation is dominated by the Antarctic Circumpolar Current (ACC) that converges towards the Chilean coast between 40 and 45°S, and separates in two branches (Figure 1b): the Peru–Chile Current (PCC) flowing towards the equator and the Cape Horn Current (CHC) moving poleward (Strub, Mesias, Montecino, Rutllant, & Salinas, 1998). Deeper currents include the Antarctic Intermediate Water (AAIW) that moves northward between ~500 and ~1,200 m water depth and the Pacific Central Water (PCW), an abyssal current that flows southward below ~1,200 m water depth (Tsuchiya & Talley, 1998). Coastal circulation along northern Patagonia changes its direction seasonally. During summer, coastal circulation is consistently equatorward as far south as 48°S, whereas during winter poleward oceanic circulation is observed next to the coast as far north as 37°S (Strub, James, Montecino, Rutllant, & Blanco, 2019).

3 | MATERIALS AND METHODS

3.1 | Stratigraphy of ODP Site 861 and sample selection

This study analyses the sedimentary sequence found at ODP Leg 141 Site 861, where three holes (A, B, and C) were drilled off the coast of southern Chile (~46°S) on the upper continental slope at 1,652 m water depth (Figure 1b). A chronological model was presented for this site based on $\delta^{18}O$ on planktonic and benthic foraminifera (Schönfeld, Spiegler, & Erlenkeuser, 1995), which indicates that the sedimentary sequence recovered at this site (200 m) represents Plio-Pleistocene strata.

At ODP site 861 we focus on the upper 80 m of the succession cored at Hole 861C because its almost complete recovery (no gaps) allows for good stratigraphic control (Behrmann et al., 1992). Strand et al. (1995) provided a description and interpretation of the lithofacies found at this site. The description that follows uses the nomenclature of Strand et al. (1995) supported by a review of the shipboard descriptions of the cores, which are posted at https://www.ngdc.noaa.gov/mgg/curator/data/joides_resolution/141/861c/visual_core_descriptions/.

Three lithostratigraphic units (I, II and III) were defined at Site 861 by shipboard sedimentologists, with Unit II further divided into two subunits, IIA and IIB (Behrmann et al., 1992). Unit I and Subunit IIA at Hole 861C constitute the cored interval investigated in this study (0–80 m; Figure 3). These were described and interpreted as follows.

Unit I (0–43.8 mbsf [meters below sea floor]) is dominated by massive to mottled silty clay to clayey silt with some nannofossils that was interpreted as hemipelagic sediments. Intervals of 10–20 cm thick composed of silty laminae grading upsection into clayey silt and silty clay represent a secondary lithofacies described near the bottom of this unit. This secondary lithofacies along with sparse laminae of silty clay to clayey silt were attributed to turbidity currents or traction transport by bottom currents (Behrmann et al., 1992; Strand et al., 1995). In addition, local 1–2 cm thick layers of silty fine sand likely represent deposits from small gravity flows (Behrmann et al., 1992).

Subunit IIA (43.8–208.9 mbsf) is composed of silty clay and clayey silt with intercalated layers of graded silt, sand and matrix- to clast-supported gravel (Behrmann et al., 1992; Strand et al., 1995). This section contains a series of muddy

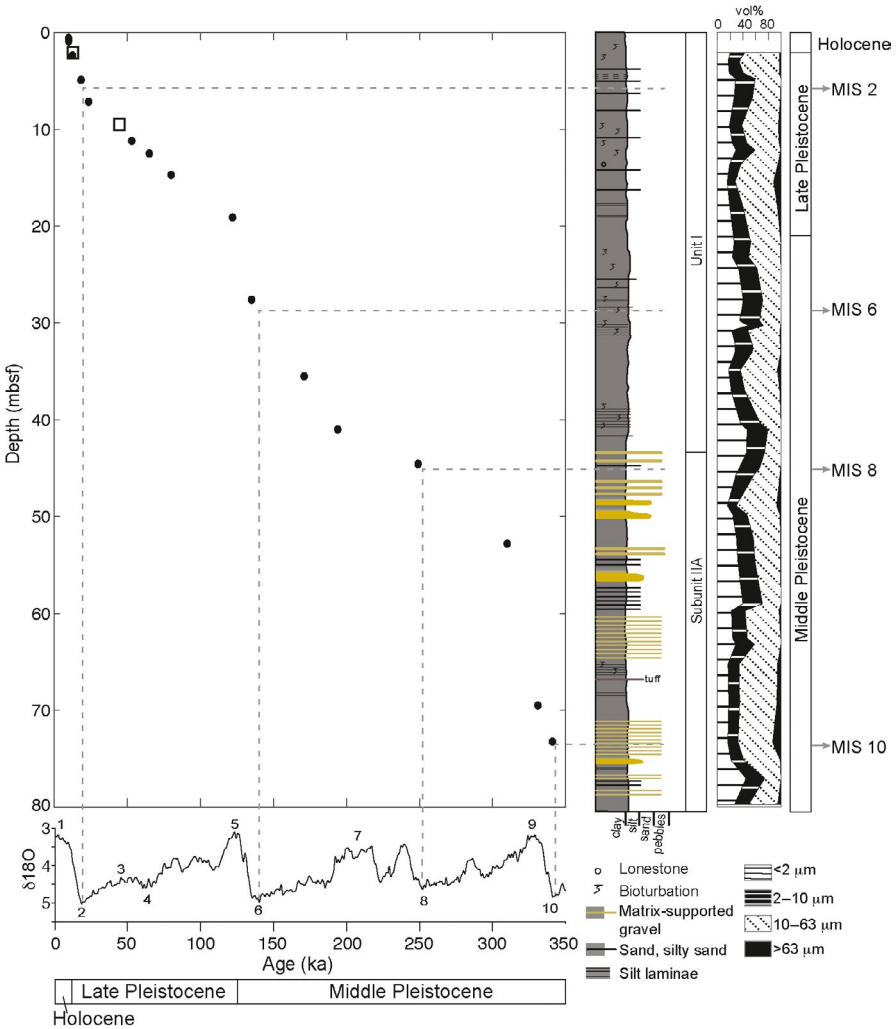

FIGURE 3 Chronological model and stratigraphy of the upper 80 m of ODP Site 861. Black dots represent chronological control points of Schönfeld et al. (1995). White squares are radiocarbon ages of this study. The chronological model is compared to the δ18O stack record of Lisiecki and Raymo (2005), where numbers along the curve mark marine isotope stages. Grey dashed lines correlate even marine isotope stages with the stratigraphic column and mark the boundary of the stratigraphic sequences identified in this site. Stratigraphic column and grain size measurements on each sample used in this study. Geological stages according to the International Stratigraphic Chart (v2018/08; www.stratigraphy.org)

gravel layers, both clast- and matrix-supported, ranging from a few centimeters to 1 m thick, with mudstone clasts ranging up to 1.7 cm maximum diameter. These were interpreted as debris flow deposits (Strand et al., 1995). Also present are 10–40 cm thick intervals comprising a basal massive sand layer followed upsection by clayey silt to silty clay, locally laminated. Following the interpretation of Strand et al. (1995), these cycles represent turbidity-flow deposits capped by hemipelagic deposits. Interbedded with these coarse lithofacies, intervals of clayey silt to silty clay locally laminated to moderately bioturbated were described.

As the main aim of this study was to perform geochemical analysis of the silt fractions, samples were selected to represent silt-bearing lithofacies in the Middle Pleistocene to Holocene interval from 0 to 80 m depth. Determination of sampling locations was guided by the shipboard core descriptions and core photographs, with the purpose to evaluate variability in sediment provenance within glacial cycles. This resulted in sample spacing ranging from 0.3 to 4.3 m (Figure 3). Note that in the following sections we simply refer to Site 861 in a general sense rather than specifying Hole 861C.

3.2 | Methodology

3.2.1 | Grain size

We evaluated sediment provenance of the silt (10–63 μm) and sand (0.063–2 mm) fractions of sediment samples from ODP Site 861 to account for potential grain-size dependency on provenance signals (e.g., Garzanti, Andò, & Vezzoli, 2009). Each of the 34 samples was air-dried and gently disaggregated manually using an agate pestle and mortar. The samples were split into several portions, of which one was used for bulk grain size analysis and another for specific grain-size separation.

The grain size distribution of 3–4 cc of bulk sediment from each sample was analysed using a Malvern Mastersizer 2000 equipped with a Hydro MV dispersion unit (Malvern Instruments Limited). Samples were not pretreated because shipboard analyses showed that the organic-matter content of the sampled section was very low (<0.5%; Behrmann et al., 1992). Each sample was passed through the Malvern cell system three times from which the average volumetric grain size distribution was obtained.

For the size fraction separation, 3–4 g of sediment were extracted, mixed with 0.05% Calgon (sodium metaphosphate solution), shaken manually for 1 min and placed in an ultrasonic bath for 25 min to ensure particle disaggregation. After 24 hr, samples were wet sieved with a 63-μm sieve. The sand-sized fraction was separated and dried in oven at 30°C for 48 hr. The 10–63 μm medium to coarse silt fraction was obtained after repeatedly centrifuging the mud solution of each sample for 15 s at 600 RPM. The clay to fine silt fractions (<10 μm) were retained but not analysed further.

3.2.2 | Sand fraction (0.063–2 mm) composition

Petrographic analyses were conducted on 24 sand samples collected from the Middle Pleistocene to Holocene interval at ODP Site 861 (0–80 m). Standard thin sections were created from sand separates and then were stained for calcium- and potassium-rich feldspar recognition using the method of Marsaglia and Tazaki (1992). Their composition was quantified using the Gazzi-Dickinson point-count method (e.g., Ingersoll et al., 1984). For each sample, 400 sand-sized poly-mineralic and mono-mineralic terrigenous and biogenic components were classified using categories defined in Marsaglia et al. (1995), including a metamorphic rock classification scheme based on Garzanti and Vezzoli (2003). Recalculated parameters were calculated to determine detrital modes and trends in compositional data.

3.2.3 | Sr and Nd composition of silt (10–63 μm) fraction

About 0.05 g of each silt fraction was weighed in acid-cleaned hex-cap Teflon vials and digested with 2 ml of Hydrofluoric acid and 1 ml of Nitric acid in an oven at 110°C. After digestion the vials were opened and the solution was dried via evaporation on a hot plate. After evaporation, 2 ml 6N of Hydrochloric acid were added to the residue and the capped vials were kept on the hot plate overnight. The next day the solution was again evaporated to dryness. Sr and Nd were separated using standard chromatographic methods (Richard, Shimazu, & Allegre, 1976). In brief, samples were loaded on BioRad AG50W-X12, 200–400 mesh cation-exchange resin in HCl medium. This step separated Rb, Sr and all of the Rare Earth Elements (REE). Nd and Sm were separated from the other REE using HCl elution on quartz columns packed with Ln-Spec resin (www.eichrom.com). Sr and Nd isotopic compositions were determined on a "Nu-Plasma" MC-ICP-MS at the Department of Geological Sciences at the University of Florida, following methods described in Kamenov, Perfit, Mueller, and Jonasson (2008). The reported $^{87}Sr/^{86}Sr$ ratios are relative to NBS 987 $^{87}Sr/^{86}Sr = 0.71024$ (± 0.00003, 2σ). The reported Nd isotopic compositions are relative to JNdi-1 $^{143}Nd/^{144}Nd = 0.512115$ (± 0.000018, 2σ).

3.2.4 | Radiocarbon dating

We tested the chronological model presented in Schönfeld et al. (1995) for ODP Site 861 by acquiring three new AMS radiocarbon dates. Mix planktonic foraminifera were separated from the >63 μm fraction of selected sediment samples and these were analysed at Beta Analytic Radiocarbon Laboratory. All radiocarbon dates were calibrated to calendar years before present (0 BP = 1950 AD) using MatCal (Lougheed & Obrochta, 2016) and the Marine13 calibration curve (Reimer et al., 2013) considering a marine reservoir age of 800 yr (Siani et al., 2013).

4 | RESULTS

4.1 | Chronology and stratigraphy

The age model proposed by Schönfeld et al. (1995) is confirmed by the radiocarbon ages determined in this study (Table 1). Figure 3 shows that radiocarbon ages fit well with the chronological model and therefore this continental slope site likely records the last 350 kyr of sedimentation, at sedimentation rates between 8 and 80 cm/kyr.

A correlation of the chronological model of ODP Site 861 with the δ18O stack record of Lisiecki and Raymo (2005) allows the identification of the main Marine Isotopic Stages (MIS; Figure 3). Since there are no local records of sea level change in the study area, we consider that sea-level cycles of the Middle to Late Pleistocene reflected in the δ18O stack record (Miller, Kominz, Browning, Wright, & Mountain, 2005; Figure 3) represent the timing of sea level change in the study area. We then correlate the even MIS

TABLE 1 Radiocarbon age of sediment samples from ODP Site 861

Lab ID	Core depth (m)	14C AMS age (yr BP)	±Error (yr)	Calibrated age (95.4% probability; cal yr BP)	Median age (cal yr BP)
Beta-483187	2.11	11,720	30	14,125–13,874	14,004
Beta-510357	9.48	41,860	620	46,866–44,509	45,603
Beta-483188	34.87	>43,500			

in the record to identify stratigraphic levels related to sea level lowstands/maximum glacial and the intervals in between these to represent full eustatic/glacial cycles. We use these levels as stratigraphic sequence boundaries (Figure 3; Catuneanu, 2006; Powell & Copper, 2002). Furthermore, given the timescale of the stratigraphic section, we consider that variations in ice proximity to the continental slope roughly coincide with global glacial/interglacial cycles (Jouzel et al., 2007).

Thus, we consider the upper 80 m at ODP Site 861 to be composed of three stratigraphic sequences reflecting full glacial cycles (Figure 3): MIS10-MIS 8, MIS 8-MIS 6 and MIS 6-MIS 4. The oldest stratigraphic sequence (MIS 10-MIS 8), corresponding to the upper section of Subunit IIA, contains a series of lithofacies that can be related to a glacial stratigraphic sequence that forms during one cycle of ice advance/retreat (Powell & Cooper, 2002). The high frequency

TABLE 2 Sr and Nd composition of marine sediment samples (10–63 μm) from ODP Site 861

Sample	Depth (mbsf)	87Sr/86Sr	±	143Nd/144Nd	±	εNd	±
1–1, 55 59	0.57	0.705814	0.000016	0.512580	0.000006	−1.13	0.03
1–2, 60 62	2.11	0.706173	0.000013	0.512555	0.000010	−1.62	0.05
1-CC, 17 21	2.69	0.706094	0.000013	0.512562	0.000009	−1.48	0.05
2–1, 121 125	4.23	0.708623	0.000012	0.512399	0.000004	−4.66	0.02
2–3, 70 74	6.72	0.708172	0.000013	0.512426	0.000004	−4.14	0.02
2–5, 56 60	9.48	0.705555	0.000013	0.512634	0.000004	−0.08	0.02
2–6, 95 99	11.37	0.705342	0.000016	0.512666	0.000006	0.55	0.03
3–1, 110 114	13.62	0.704964	0.000013	0.512710	0.000006	1.40	0.03
3–3, 17 21	15.39	0.704939	0.000009	0.512720	0.000004	1.60	0.02
3–4, 95 99	17.92	0.706886	0.000010	0.512473	0.000004	−3.22	0.02
3–7, 15 19	21.47	0.705567	0.000012	0.512630	0.000006	−0.16	0.03
4–2, 85 89	24.37	0.705150	0.000010	0.512678	0.000003	0.78	0.02
4–4, 115 119	27.67	0.706140	0.000013	0.512542	0.000004	−1.87	0.02
4–6, 28 32	29.7	0.707152	0.000012	0.512481	0.000008	−3.06	0.04
4–6, 125 129	30.67	0.705772	0.000011	0.512584	0.000006	−1.05	0.03
5–2, 50 54	32.32	0.706315	0.000014	0.512525	0.000006	−2.20	0.03
5–4, 5 9	34.87	0.708615	0.000010	0.512381	0.000007	−5.01	0.03
5–5, 70 74	37.02	0.705615	0.000012	0.512611	0.000005	−0.53	0.03
5–7, 110 114	40.42	0.706672	0.000013	0.512527	0.000005	−2.17	0.03
6–2, 90 94	43.42	0.705912	0.000009	0.512564	0.000006	−1.44	0.03
6–4, 10 14	45.52	0.706195	0.000011	0.512539	0.000006	−1.93	0.03
6–6, 35 39	48.77	0.706593	0.000010	0.512507	0.000005	−2.56	0.03
6–7, 65 69	49.07	0.705775	0.000012	0.512593	0.000007	−0.88	0.03
7–2, 72 76	52.74	0.705532	0.000017	0.512652	0.000008	0.27	0.04
7–3, 116 120	54.68	0.704859	0.000011	0.512732	0.000004	1.83	0.02
7–7, 21 25	58.25	0.705617	0.000010	0.512624	0.000005	−0.27	0.03
8–2, 105 109	62.57	0.705717	0.000013	0.512594	0.000005	−0.86	0.03
8–3, 15 19	63.17	0.705447	0.000013	0.512630	0.000005	−0.16	0.02
8–4, 71 75	65.08	0.705326	0.000011	0.512637	0.000005	−0.02	0.02
8–7, 15 19	69.02	0.705298	0.000013	0.512656	0.000008	0.35	0.04
10–2, 78 82	73.3	0.705618	0.000011	0.512597	0.000004	−0.80	0.02
10–3, 111 115	75.13	0.705805	0.000010	0.512614	0.000005	−0.47	0.03
10–5, 10 14	77.02	0.706364	0.000013	0.512526	0.000006	−2.18	0.03
10-CC, 20 24	79.52	0.706082	0.000014	0.512552	0.000006	−1.68	0.03

Note: Sample numbers represent core-section and depth interval of the sample.
Depth was calculated at the mid-point of each sample interval.
εNd = [(143Nd/144Nd)sample/(143Nd/144Nd)CHUR − 1] × 104 with 143Nd/144Nd (CHUR) = 0.512638 (Jacobsen & Wasserburg, 1980).

of gravity-flow deposits (debris flows and turbidites) reflects high sediment supply to the continental margin (Figure 3). The two stratigraphic sequences that form Unit I represent two full glacial cycles -MIS 8-MIS 6 and MIS 6-MIS 4- do not show coarse lithofacies that could be related to glacial system tracts. Instead, these two sequences are formed by hemipelagic sedimentation and sparse gravitational flow events (Strand et al., 1995). Since there is no clarity on the extension of the western flank of the PIS during the past glacial cycles, or the magnitude of Pleistocene isostatic adjustment of the continental crust to ice load in the study area (e.g., Dietrich et al., 2010), we prefer to interpret the stratigraphy of Site 861 as reflecting the combined influence of changes in sea level and sediment supply in response to ice dynamics in Patagonia. The marked change in the lithofacies succession between Subunit IIA and Unit I indicates an important change in the sedimentary processes forming continental slope strata during the Middle Pleistocene.

4.2 | Grain size analysis

The grain size analyses supports previous observations on this site of limited variation of grain size (Diemer & Forsythe, 1995). The middle to coarse silt size fraction (10–63 μm) dominates the samples of this study, ranging from 21 to 64 vol% (median 47 vol%), followed by clay and fine silt (median 26 and 25%vol, respectively; see Table S1 for full grain size dataset). Sand represents a very minor proportion of the samples ranging from 0 to 13 vol% (median 1.1 vol%). The variability in the proportion of these grain size fractions in relation to the stratigraphy is presented in Figure 3.

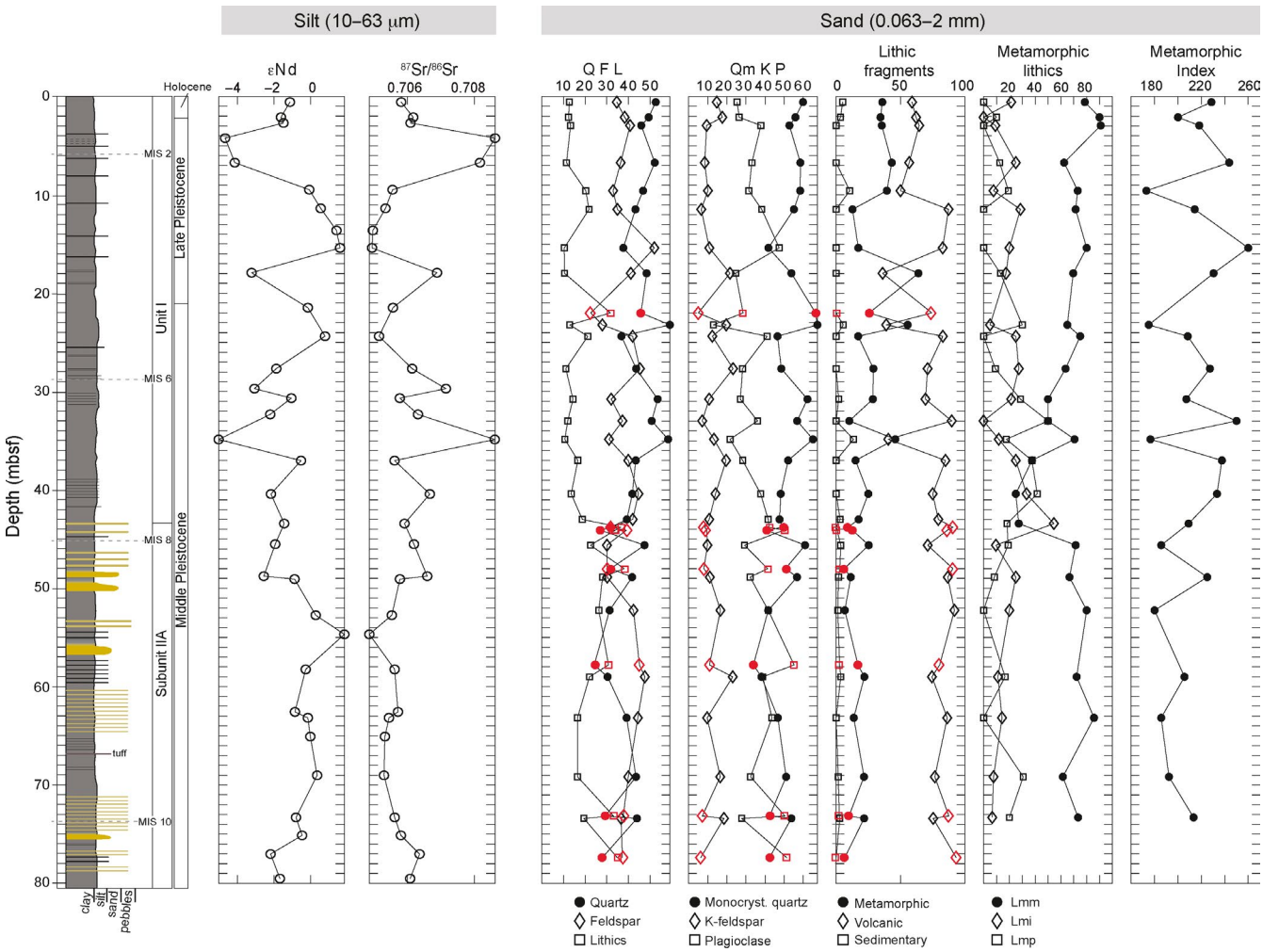

FIGURE 4 Stratigraphic column of the upper 80 m of ODP Site 861 compared to Sr and Nd isotopic composition of the silt fraction (10–63 μm) and various composition parameters of the sand fraction (0.063–2 mm). Grey dashed lines mark the boundaries of the stratigraphic sequences identified in this site. $\varepsilon Nd = [(143Nd/144Nd)sample/(143Nd/144Nd)CHUR - 1] \times 10^4$ with 143Nd/144Nd (CHUR) = 0.512638 (Jacobsen & Wasserburg, 1980). See Table 2 for details on the isotopic results. In the sand fraction. Lmm: metamorphic lithic fragment with psammitic protolith, Lmi: metamorphic lithic fragment with igneous protolith, Lmp: metamorphic lithic fragment with pelitic protolith. The sand compositional data of Marsaglia et al. (1995) are included in red. See Table S3 for detailed results of the compositional analysis of the sand fraction

TABLE 3 Sand recalculated parameters used for provenance analysis of sediment from ODP Site 861

Sample[a]	Depth (mbsf)[b]	QFL%Q	QFL%F	QFL%L	QmKP%Qm	QmKP%K	QmKP%P	L%Lm	L%Lv	L%Ls	Lm% Lmm	Lm% Lmi	Lm% Lmp	I%	II%	III%	IV%	Metamorphic Index
1-1, 55 59	0.57	49.2	32.4	18.3	59.8	14.8	25.4	23.3	73.3	3.3	78.6	21.4	0.0	7.1	57.1	35.7	0.0	229
1-2, 60 62	2.11	46.2	35.9	17.9	55.9	17.6	26.5	22.2	75.6	2.2	90.0	0.0	10.0	30.0	40.0	30.0	0.0	200
1-CC, 17 21	2.69	42.3	37.5	20.2	52.7	9.5	37.8	21.6	78.4	0.0	90.9	9.1	0.0	18.2	45.5	36.4	0.0	218
2-3, 70 74	6.72	49.6	34.6	15.8	58.5	8.5	33.1	29.6	70.4	0.0	62.5	25.0	12.5	6.3	43.8	50.0	0.0	244
2-5, 56 60	9.48	42.7	30.1	27.2	58.4	10.1	31.5	26.8	66.0	7.2	73.1	7.7	19.2	30.8	65.4	3.8	0.0	173
2-6, 95 99	11.37	36.6	29.5	33.9	55.1	6.6	38.3	6.9	93.1	0.0	71.4	28.6	0.0	14.3	57.1	28.6	0.0	214
3-3, 17 21	15.39	34.9	48.2	16.9	41.8	10.8	47.4	9.8	90.2	0.0	80.0	20.0	0.0	0.0	40.0	60.0	0.0	260
3-4, 95 99	17.92	46.6	39.6	13.8	53.8	21.6	24.6	46.9	53.1	0.0	69.6	17.4	13.0	8.7	56.5	30.4	4.3	230
4-1, 120 124	23.22	56.7	26.8	16.5	67.4	19.7	13.0	41.7	54.2	4.2	65.0	5.0	30.0	45.0	35.0	20.0	0.0	175
4-2, 85 89	24.37	31.7	36.1	32.2	46.5	12.4	41.1	9.8	90.2	0.0	75.0	25.0	0.0	25.0	41.7	33.3	0.0	208
4-4, 115 119	27.67	40.6	42.2	17.2	48.5	23.3	28.2	17.5	82.5	0.0	63.6	27.3	9.1	9.1	54.5	36.4	0.0	227
4-6, 125 129	30.67	49.2	29.5	21.4	62.2	10.8	27.1	17.7	81.0	1.3	50.0	21.4	28.6	28.6	35.7	35.7	0.0	207
5-2, 120 124	33	46.2	33.9	19.9	56.8	7.1	36.1	5.6	94.4	0.0	50.0	0.0	50.0	0.0	50.0	50.0	0.0	250
5-4, 5 9	34.87	56.1	29.8	14.1	65.0	13.3	21.7	33.3	56.9	9.8	70.6	11.8	17.6	41.2	41.2	17.6	0.0	176
5-5, 70 74	37.02	38.5	35.5	26.0	52.1	19.6	28.3	8.6	91.4	0.0	37.5	25.0	37.5	12.5	37.5	50.0	0.0	238
5-7, 110 114	40.42	38.2	40.8	20.9	48.2	14.1	37.7	14.8	85.2	0.0	25.0	33.3	41.7	16.7	33.3	50.0	0.0	233
6-2, 90 94	43.42	34.6	37.0	28.3	47.6	10.8	41.6	10.2	88.0	1.9	27.3	54.5	18.2	27.3	36.4	36.4	0.0	209
6-4, 10 14	45.52	41.0	26.0	33.0	60.9	9.9	29.2	14.9	83.0	2.1	71.4	9.5	19.0	38.1	38.1	23.8	0.0	186
6-6, 35 39	48.77	33.6	24.4	42.0	56.7	11.1	32.2	6.2	92.8	1.0	66.7	25.0	8.3	25.0	33.3	33.3	8.3	225
7-2, 72 76	52.74	25.6	34.6	39.8	41.7	16.7	41.7	3.6	95.6	0.7	80.0	20.0	0.0	40.0	40.0	20.0	0.0	180
7-7, 21 25	58.25	26.3	41.3	32.4	38.1	23.1	38.8	12.9	84.9	2.2	72.2	11.1	16.7	22.2	50.0	27.8	0.0	206
8-3, 15 19	63.17	34.6	39.1	26.3	46.7	9.7	43.6	7.6	92.4	0.0	85.7	14.3	0.0	42.9	28.6	28.6	0.0	186
8-7, 15 19	69.02	38.6	35.5	25.9	51.0	16.6	32.4	12.3	86.8	0.9	61.5	7.7	30.8	23.1	61.5	15.4	0.0	192
10-2, 78 82	73.3	38.7	32.3	29.0	53.7	18.5	27.8	12.8	85.5	1.7	73.3	6.7	20.0	20.0	46.7	33.3	0.0	213

Note: The calculation of these parameters can be found in Table S2.

Ranks I, II, III, IV refers to a metamorphic grain classification scheme in Garzanti and Vezzoli (2003).

[a]Sample numbers represent core-section and depth interval of the sample.

[b]Depth was calculated at the mid-point of each sample interval.

4.3 | Sr and Nd isotopic composition of the silt fraction (10–63 μm)

Sr and Nd isotope compositions of the 10–63 μm size fraction of the sediment samples show a wide range of values ($^{87}Sr/^{86}Sr$: 0.7049 to 0.7086; εNd: −5.013 to 1.834; Table 2). Samples from Subunit IIA show a limited range of variability in both isotopic systems ($^{87}Sr/^{86}Sr$: 0.7049 to 0.7067; εNd: −2.555 to 1.834), compared to Unit I that exhibit a wider range of values ($^{87}Sr/^{86}Sr$: 0.7049 to 0.7086; εNd: −5.013 to 1.6; Figure 4).

The stratigraphic sequence in Subunit IIA shows a progressive change in isotopic composition that is reflected in relatively high εNd and low $^{87}Sr/^{86}Sr$ values followed upsection by lower εNd and higher $^{87}Sr/^{86}Sr$ values. The two stratigraphic sequences in Unit I do not show any specific compositional trend (Figure 4).

4.4 | Sand composition

Petrographic analyses of the sand fraction show that it is dominated by quartz (30%–59%) and feldspar (28%–52%) followed by lithic fragments (10%–28%; Table 3, Figure 4). Quartz is mainly the monocrystalline variety (Qm:Qp = 35:1). Feldspars are dominated by plagioclase (mean values of Plagioclase:K-feldspar = 21:9). Other monomineralic components include minor micas (biotite and muscovite) and heavy minerals (mostly pyroxene, amphibole and epidote grains; see Table S2 for full raw point count dataset). Volcanic (with vitric, felsitic, microlitic and lathwork textures) and metamorphic lithics dominate the lithic fragment portion of the samples, with minor sedimentary (argillite-shale, siltstone) fragments (mean values of Lv:Lm:Ls = 71:27:2). Metamorphic lithic fragments are largely dominated by sedimentary protoliths (Lmm, Lmp) with minor igneous (Lmi) protoliths (mean values of Lmm:Lmi:Lmp = 66:18:16). The metamorphic grade of these grains falls within ranks I, II and III of metamorphic fragments defined by Garzanti and Vezzoli (2003; Table 3) that correspond to rock of very low and low metamorphic grade. Intrabasinal biogenic grains (Bio) include calcareous (foraminifera) and siliceous (diatoms, sponge spicules, radiolarians) microfossils ranging from 0% to 38% (median 13%).

Samples from Unit I tend to have a broader compositional variability than those from Subunit IIA (Figure 4). Unit I is enriched in quartz compared to Subunit IIA, which in contrast tends to have a relatively high concentration of feldspar (plagioclase). Volcanic lithic fragments largely dominate both Unit I and Subunit IIA with metamorphic rock fragments increasing up section in Unit I. Also, the Metamorphic Index (MI), a measure of the average metamorphic grade of the lithic fragments in the samples (Garzanti & Vezzoli, 2003), shows more variability in Unit I than in Subunit IIA reaching higher values in the former unit.

5 | DISCUSSION

The formation of the continental slope sedimentary sequence at Site 861 was influenced by dynamics of the PIS (Behrmann et al., 1992; Kilian & Behrmann, 2003; Schönfeld et al., 1995; Strand et al., 1995). Therefore, it is likely that the differences observed in the stratigraphic characteristics of Subunit IIA and Unit I are a response to variations in the mode that the PIS produced and transferred sediment to the continental margin during the Middle to Late Pleistocene. Variations in the sediment provenance signature of these two lithostratigraphic units point to a change in the erosion pattern of the PIS during this period. In the following discussion, we will reconcile sediment provenance and stratigraphy to reconstruct erosion patterns and sediment transfer to the ocean in a glacially influenced environment.

5.1 | Patterns of glacial erosion

The geomorphic analysis of North Patagonia carried out by Glasser and Jansson (2005) identified the absence of scoured bedrock in the central area of the northern PIS (during the Last Glacial Maximum, LGM), suggesting non-erosive conditions beneath ice divides (Boulton & Clark, 1990). We accept the ice divide of the PIS as reconstructed by Glasser and Jansson (2005) and Glasser et al. (2008) and therefore evaluate potential sediment provenance signals from west of that boundary.

5.1.1 | Sand provenance using detrital modes

Previous workers looked at the composition and provenance of sand-rich gravity-flow deposits at ODP Site 861 (Marsaglia et al., 1995). However, the sand-size fraction represented a very small portion of the sediment samples of this study, which may have been delivered by different processes to the site. We therefore first compare the two datasets (Figure 4). Sandy gravity-flow deposits described in Marsaglia et al. (1995; marked red in Figure 4) are relatively enriched in lithic fragments and feldspars compared to sand fractions from samples analysed in this study. However, the sand samples from the two datasets are dominated by plagioclase and monocrystalline quartz and share similar trends in the types of lithic fragments. Therefore, any difference in the sedimentary processes that delivered sand within the coarse and fine lithofacies of Site 861 did not result in different provenance signals.

Variability in the composition of the sand fraction of the samples of this study provides relevant information on sediment provenance. Sand composition dominated by quartz (Qm) and feldspars indicates that sand originates from the combined erosion of the Patagonian Batholith and the CMC. The dominance of volcanic fragments in the lithic fraction is consistent with previous observations in sites of ODP Leg 141 expedition (Heberer et al., 2010; Marsaglia et al., 1995). It is likely that volcanic fragments originated from the Hudson volcano (Marsaglia et al., 1995; Strand et al., 1995), the closest volcanic centre to the drill site (Figure 2), which has been volcanically active during the last 1 Myr (Orihashi et al., 2004). Even though volcanoes and associated volcanic deposits represent a minor portion of the study area (Figure 2), the release of pyroclastic fragments to the atmosphere during volcanic eruptions (e.g., Carel et al., 2011) and the relatively easy erosion of volcanic deposits (e.g., Heberer et al., 2010) may have favoured the transfer of volcaniclastic material to the nearby continental slope. A decrease in volcaniclastic material up section, and in particular of vitric volcanic lithic fragments, testify for reduced basin connectivity with the inner portion of the Patagonian Andes with time.

Metamorphic lithic grains (Lm) as well as mica are minor components in the sand fraction suggesting limited erosion of the CMC and dilution by volcaniclastic material during volcanic paroxysm. However, the progressive up section variability of the MI value indicates a temporal evolution of the areas of the CMC under erosion. Relatively lower MI values in Subunit IIA suggest erosion of parts of CMC with low metamorphic grade, and more variable and some high values in Unit I suggests mixed erosion of low to medium metamorphic grade rocks of CMC. Following the description of Hervé et al. (1981) of the CMC, this represents preferential erosion of the Eastern belt of the CMC during accumulation of Subunit IIA and expansion of erosion towards the Western belt of this complex during accumulation of Unit I. Moreover, higher variability in MI values suggests more disorganized erosion of the CMC during accumulation of Unit I, suggesting a re-organization of PIS ice flow and expansion of its cover over time.

5.1.2 | Silt provenance using geochemical analyses

Smear-slide analysis of the silt fraction by shipboard scientists showed siliciclastic components similar to those found in the sand fraction, including: quartz, feldspar, metamorphic rock fragments, volcanic debris, mica, chlorite, epidote, pyroxene and amphibole (Behrmann et al., 1992). Therefore it is not surprising that Sr and Nd values of the silt size fraction of ODP Site 861 samples fall well within the range of isotopic composition of bedrock types in the study area (Figure 5).

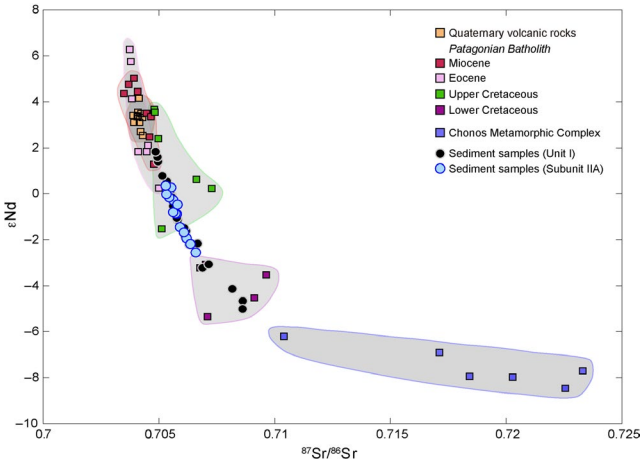

FIGURE 5 Sr and Nd isotopic signature of main lithological units of northern Patagonia compared to the isotopic signatures of sediment samples from ODP Site 861. Bedrock Sr and Nd data from Weaver, Bruce, Nelson, Brueckner, and LeHuray (1990), Lopez-Escobar, Kilian, Kempton, and Tagiri (1993), and Pankhurst et al. (1999)

Samples show a marked dominance of the Patagonian Batholith as a source of sediment, which is consistent with previous provenance results of offshore sediments in samples from Leg 141 sediment cores based on similar isotopic analyses (Kilian & Behrmann, 2003). The lack of a strong signal from the CMC, the closest potential bedrock source to Site 861, suggests overall spatially restricted erosion of it during the Middle - Late Pleistocene in northern Patagonia (Thomson et al., 2010). This indicates that the ice streams draining the PIS focused on a specific region of northern Patagonia.

The restricted compositional variation of samples from Subunit IIA is compatible with a source in the Lower and Upper Cretaceous rocks of the Patagonian Batholith (Figure 5). The stratigraphic sequence that comprises most of Subunit IIA shows a progression in its sediment provenance signal from a widespread erosion of Cretaceous rocks of the Patagonian Batholith in the lower half (ice growth/sea level fall) to a signal with likely more participation of Lower Cretaceous rocks in the upper section (ice maximum extent/lowest sea level; Figure 4). This restricted signal is still active during the formation of the overlying stratigraphic sequence, which can be interpreted as reworking of stored sediment as the ice rapidly retreated and sea level rose during the following glacial cycle.

Unit I is characterized by a broader compositional signature of the two stratigraphic sequences, which is compatible with sediment sourced in the Cretaceous and Miocene portions of the Patagonian Batholith (Figure 5). We disregard any significant influence of Eocene rocks of the Patagonian Batholith since they represent a minimal portion of the study area (Figure 2). Very low εNd and high $^{87}Sr/^{86}Sr$ values for some samples of Unit I suggest some influence of the CMC in the sediment that is not evident in samples from Subunit IIA (Figure 5). A minor

influence of the CMC on the provenance signal of the silt-size fraction may be related to partial ice-sheet cover of this region during the past glaciations. This is consistent with a previous paleoclimate reconstruction in the area, which found that some areas of coastal Patagonia may have been ice-free during the last glaciation (Montade et al., 2013).

The influence of the Patagonian Batholith on sediment input offshore of Patagonia has been previously analysed by Heberer et al. (2011). Based on apatite fission track data from ODP Site 860 core sediment samples (Figure 1b), they found a dominant influence of a Miocene source, with a secondary population ranging from Eocene to Early Cretaceous age. This points to erosion focused on Miocene intrusions within the Batholith during the Pleistocene (Heberer et al., 2011). The absence of a strong Miocene signal in the isotopic signature of the silt size fraction in this study may be related to differences in the grain size analysed (sand-size apatite in Heberer et al., 2011) and the stratigraphic resolution of both studies, for which this research investigates provenance over the last few glacial cycles vs. million-year scale erosional signals.

Regardless of these discrepancies, there is a strong signal of erosion of the Patagonian Batholith throughout the sedimentary succession of this study, which is consistent with the area of highest rates of exhumation during the Cenozoic (Thomson et al., 2010) and roughly aligns to the modelled hotspot of erosion of the last 2 Myr in Patagonia (Herman & Brandon, 2015). Herman and Brandon (2015) argued that the migration of zone of maximum precipitation to around 44°S during Pleistocene glaciations led to high ice discharge and therefore sliding rates of the PIS, enhancing glacial erosion. Peak precipitation rates are found in the interior of the continent where the mountain range is relatively high (for example, Figure 1a) that could explain focused erosion of the Patagonian Batholith. In addition, the Patagonian Batholith is affected by the LOFZ (Figure 1b), representing a zone of weak bedrock that could have facilitated glacial erosion in the core of the Andes.

At the glacial–interglacial timescale, there are clear differences in the sediment provenance signal between Subunit IIA and Unit I, progressing from a source area that was spatially constrained to one with more spatially variable erosion. Even though the portion of Subunit IIA included in this study represents only one complete glacial cycle, the rapid and marked shift in provenance signal in Unit I indicates a change in ice dynamics during the Middle to Late Pleistocene that promoted rapid fluctuations and expanded erosion towards the west.

5.2 | Sedimentary processes and glacial erosion in Patagonia

The stratigraphic sequence in Subunit IIA, between MIS 10 and MIS 8, represents a full cycle of high to low sea level (Figure 3) and progressive proximity of the ice margin to the continental slope that promotes the accumulation of coarse lithofacies on it (Powell & Copper, 2002). Mud clasts present in the debris-flow deposits of this stratigraphic sequence (Behrmann et al., 1992) suggests reworking of sediment accumulated in fjords, channels and/or coast, or erosion of semi-consolidated continental slope sediment during downslope sediment transport. In contrast, the two overlying stratigraphic sequences of Unit I, formed during the sea level/ glacial cycle of MIS 8–MIS 6 and MIS 6–MIS 2, contain very few and fine-grained gravity flow deposits in lower and upper intervals separated by a middle interval of hemipelagic mud (Figure 3). This is related to a more distal influence of sediment evacuation from the PIS to Site 861. The formation of these gravity-flow deposits may be related to periods of increased PIS activity (advance and retreat) that promoted overall increased sediment supply to the continental margin and gravity flows in the continental slope. The current configuration of the continental margin with multiple gullies (Figure 1b) likely conveys gravity flows of reduced volume and limited depositional extent (Thornburg & Kulm, 1987) that are represented by the gravity flow deposits of Unit I.

The dominance of coarser gravity flow deposits in Subunit IIA suggests that sediment supply to the continental margin near Site 861 was relatively high for which it is likely that the PIS was eroding the core of the Patagonian Andes and efficiently transferring the material to the continental margin during the cycle MIS 10–MIS 8. The metamorphic signal in the sand-size fraction of this interval points to erosion of the eastern metamorphic belt that is in contact with the Patagonian Batholith (Figure 2). This indicates that the PIS did not expand over the entire CMC and likely reached the continental margin through outlet glaciers flowing along fjord valleys that sustained high sediment supply to the ocean (Figure 6). The complex geometry of the fjords and channels in the study area likely contributed to confining the flow of ice towards the ocean. Ice flow along zones of weakened bedrock may have produced areas of preferential erosion, promoting topographic control of ice stream flow (Glasser & Ghiglione, 2009), and therefore restricting the suite of rocks under glacial erosion. Models of the LGM ice sheet in the study area show outlet glacier velocities of 400 m/yr in the western fjords (Hulton et al., 2002), suggesting that fast-flowing outlet glaciers could have rapidly transferred sediment towards the margins of the PIS (Hubbard et al., 2005), In such scenario, it is likely that an ice stream transported sediment northward along the Moraleda Channel (Figure 6), transferring sediment with a more important Miocene signal in that direction. The Moraleda Channel is deep (400 m maximum depth; Rodrigo, 2008) and was excavated into the sedimentary Traiguén Formation (Encinas et al., 2016), where a branch of the LOFZ is located, favouring ice flow given the

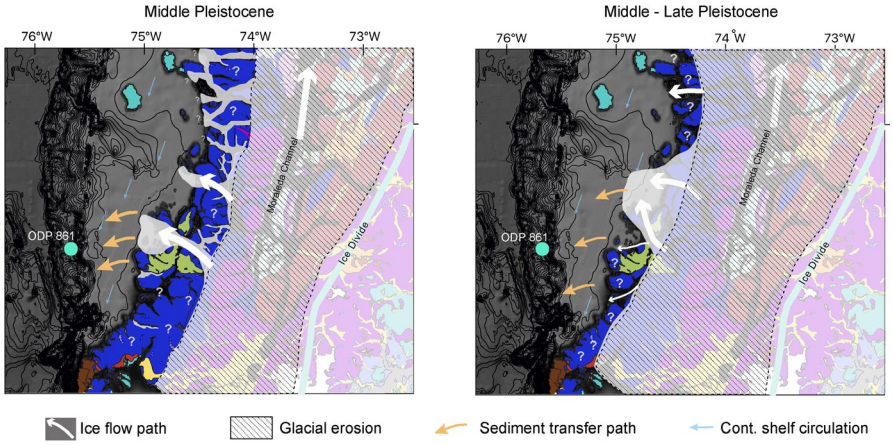

FIGURE 6 Conceptual model representing erosion patterns and sediment transfer to the continental margin during the Middle to Late Pleistocene in northern Patagonia. Ice extent to the west is limited to the interpreted area under glacial erosion since there is no additional evidence to support ice extension further to the west. Thickness of the ice flow path arrows is proportional to possible rate of ice export. Considering the analogy between austral summer/winter atmospheric conditions and glacial/interglacial climate presented in Lamy et al. (2010), we model a dominant poleward coastal circulation during the Middle-Late Pleistocene given that cold conditions are prevalent ~90% of the time (Tzedakis et al., 2009). Since this investigation focuses on the material delivered to the west of the ice divide, we do not make inferences on glacier erosion east of this boundary. To see this figure in colours, please consult the online version of this manuscript

relatively low resistance of sedimentary rocks, amplified by the weakness zone produced by the fault system.

The provenance signal of Unit I suggests a complex pattern of erosion over a more extended region of northern Patagonia, including parts of the Western belt of the CMC and Miocene rocks of the Patagonian Batholith. The analysis of seismic facies in the fjord region of northern Patagonia provides evidence of glacial deposits around the outlet of fjords (DaSilva et al., 1997). These deposits have been interpreted to form during the last glacial cycle, suggesting that the PIS had some expansion towards the continental shelf during this period (DaSilva et al., 1997). A more expansive PIS during glacial periods may have favoured the formation of larger drainage networks within the ice sheet (e.g. Stokes, Margold, Clark, & Tarasov, 2016) that the provenance signal indicates were highly dynamic, promoting the erosion of changing parts of the landscape. The formation of fast-flowing warm-based erosive ice in fjords may have been surrounded by slow-flowing cold-based protective ice on the surrounding bedrock (Briner, Miller, Davis, & Finkel, 2006; Briner, Miller, Finkel, & Hess, 2008; Jamieson, Sugden, & Hulton, 2010) explaining the minor provenance signal from the CMC. Alternatively, thin ice cover on the fjord region of the CMC may have hampered erosion of this lithological unit, except for the deep fjord and channels (Briner et al., 2006).

The reconciliation of expanding and changing PIS dynamics and the fine-grained lithofacies of Unit I requires a change in the flow dynamics of the outlet glaciers and the pattern of sedimentation in the continental margin. According to the model of Hubbard et al. (2005) and geomorphological mapping by Glasser and Jansson (2005) and Glasser et al. (2008), ice flow in the PIS during the LGM comprised several ice streams that delivered sediment to the northwest, which is consistent with the general orientation of the fjords and channels in the study area (Figure 6). Considering the bathymetry of the study area (Figure 2), we speculate that ice discharge could occur through a major ice stream flowing northwestward along a modern shelf-edge embayment, north of Site 861 during the formation of Unit I (MIS 8–MIS 2; Figure 6). This ice stream could have been key in reducing sediment input to the continental margin near Site 861 by diverting sediment supply to another region of the continental slope. Therefore, suspended sediment moving southward along the coastal currents would be the dominant sediment dispersal mechanism to ODP Site 861 during the formation of Unit I (Figure 6).

5.3 | Glaciological implications

We have argued that an important change in PIS dynamics in northern Patagonia occurred during the transition from MIS 8 to MIS 7. However, the mechanisms that could have led to an expansion and reorganization of PIS erosive patterns during the last two glacial cycles are unclear.

There is evidence on the eastern side of the PIS ice divide of a regionally significant glaciation during MIS 8 (maximum extent at 260–270 ka, Hein et al., 2017). This is consistent with sea-surface temperature records from offshore Patagonia that show a long and cold glaciation during MIS 8 (Ho et al., 2012). However, provenance data from this study suggests that during MIS 8 erosion focused largely on the Patagonian Batholith with only partial erosion of the Eastern belt of the CMC, suggesting limited ice cover on the CMC. Therefore, it can be argued that the

spatial extension of the PIS, at least during MIS 8, was not symmetrically extensive between its western and eastern sides. Extensive ice growth during MIS 8 may have been spatially limited to the west due to fast ice flow along existing channels and fjords, like the Moraleda Channel to the north or channels draining ice to the west (Figure 6). This could have limited the areas under glacial erosion, as reflected in the sediment provenance signal, as well as promoted high sediment input to the continental margin and accumulation of coarse lithofacies on the continental slope.

The lithostratigraphic transition between Subunit IIA and Unit I occurred after the coldest peak of MIS 8 and initiation of the mild interglacial of MIS 7 (Jouzel et al., 2007). A mild interglacial during MIS 7 may have led to a partial melting of the PIS, which was followed by renewed ice growth during MIS 6 that promoted its expansion and reorganization of the drainage system. Indeed, sediment provenance suggests that larger areas of northern Patagonia were covered by ice compared to the previous glaciation. However, observations of glacial deposits in the eastern side of PIS show that, for example, the glaciation of MIS 6 was not as extensive as MIS 8 (Hein et al., 2017), which, in turn, supports the idea of no correlation between the lateral extension of the western and eastern flanks of PIS during glaciations. Moreover, the provenance signal in Unit I suggests that outlet glacier flow in the west flank of PIS was re-organized and probably had a lower degree of structural control as inferred during deposition of Subunit IIA. Even though the provenance signal is still dominated by the Patagonian Batholith, the high provenance variability within Unit I suggests a fluctuating sediment supply system. The finer-grained lithofacies of Unit I indicates that sediment delivery occurred more distal from ODP Site 861, suggesting that sediment transfer paths to the continental slope also changed during the Middle to Late Pleistocene.

A contentious idea is the non-climatic control on ice extent and associated patterns of erosion, in which moraine deposits of early glaciations were deposited farther down valley compared to more recent glaciations (Anderson, Dühnforth, Colgan, & Anderson, 2012; Kaplan et al., 2009). In this case, glacier deposits accumulated closer to the continental shelf during formation of Subunit IIA may explain the relatively coarse lithofacies accumulated in the continental slope during the Middle Pleistocene. Deepening of the glacial valleys after successive glaciations could have led to limited extension of outlet glaciers on to the continental shelf during the last two glaciations (Kaplan et al., 2009), reducing the overall supply of sediment to the continental margin. The overdeepening of valleys would promote a decrease in accumulation relative to ablation, and the adjustment of the subglacial drainage network. Further seismic, bathymetric and sedimentological surveys of the Chilean Patagonian continental margin and fjords, as well as detailed geomorphological analysis of the region, including cosmogenic dating and ice-sheet modelling, are needed to better reconstruct PIS dynamics, erosion and sediment transfer to the ocean.

6 | CONCLUSIONS

This work investigates the link between glacial erosion in the northern Patagonian Andes and offshore sedimentation during the Middle-Late Pleistocene. Sediment provenance analysis of the sand and silt-size fraction of the sediment and a revision of the stratigraphy of ODP Site 861 on the Pacific continental slope offshore of Patagonia shows that erosion patterns of the Patagonian Andes and sediment transfer to the ocean have changed during this period.

Sediment provenance is dominated by erosion of the Patagonian Batholith that corresponds to the core of the Patagonian Andes, whereas the provenance signal of the more proximal sediment source, the CMC, is very minor and better distinguished in sediment accumulated during the last two glaciations. This indicates that the PIS has mostly focused glacier erosion on the axis of the Patagonian Andes. This area co-exists with the zone of weak bedrock within the Liquiñe-Ofqui Fault Zone and very high precipitation patterns, suggesting that the distribution of glacial erosion may be influenced by structural and/or climatic controls.

Changing characteristics of the stratigraphic succession from Middle to Late Pleistocene are coincident with a shift in the character of the provenance signal. Before the MIS 8/7 transition (240 kyr) erosion was focused on a restricted region of the Patagonian Batholith and sediment efficiently transferred to the continental slope, producing a succession of coarse lithofacies that are expected in continental margins influenced by the activity of an ice sheet. After the MIS 8/7 transition, the stratigraphic sequence is dominated by a succession of fine-grained lithofacies that reflect a shift in the mode of sediment dispersal in the continental margin, with an inferred more distal influence of ice-sediment discharge. The provenance signal of this interval fluctuated rapidly indicating the influence of additional sources of sediment and erosion over a larger extent of the landscape. This suggests more complex PIS dynamics during the last two glaciations that likely resulted in a reorganization of ice streams and outlet glacier flow paths that diverted sediment transfer far from Site 861.

ACKNOWLEDGEMENTS

This research used samples and data provided by the International Ocean Discovery Program (IODP). We thank Gabriel Vargas and Christian Nievas of the Sedimentology

Laboratory (Universidad de Chile) for facilitating sediment sample processing. We thank the Associate Editor Cari Johnson, Nicholas Roberts and an anonymous reviewer for their helpful suggestions. This project was funded by CONICYT-FONDECYT postdoctoral fellowship #3170611 to T. Villaseñor. T. Villaseñor acknowledges support from the Millennium Science Initiative of the Ministry of Economy, Development and Tourism of Chile, grant Núcleo Milenio Paleoclima.

DATA AVAILABILITY STATEMENT

The data that support the findings of this study are provided in the supplementary material.

ORCID

Tania Villaseñor https://orcid.org/0000-0002-8353-3130
Daniel Tentori https://orcid.org/0000-0002-4681-5163
Luisa Pinto https://orcid.org/0000-0002-2176-2958

REFERENCES

Anderson, R. S., Dühnforth, M., Colgan, W., & Anderson, L. (2012). Far-flung moraines: Exploring the feedback of glacial erosion on the evolution of glacier length. *Geomorphology*, *179*, 269–285. https://doi.org/10.1016/j.geomorph.2012.08.018

Behrmann, J. H., Lewis, S. D., Musgrave, R. J., Arqueros, R., Bangs, N. L., Boden, P., … Forsythe, R. (1992). Site 861. *Proceedings of the ocean drilling program, initial reports* (Vol. *141*, pp. 239–299). College Station, TX: Ocean Drilling Program.

Bertrand, S. B., Hughen, K. A., Sepúlveda, J., & Pantoja, S. (2012). Geochemistry of surface sediments from the fjords of Northern Chilean Patagonia (44–47°S): Spatial variability and implications for paleoclimate reconstructions. *Geochimica Et Cosmochimica Acta*, *76*, 125–146. https://doi.org/10.1016/j.gca.2011.10.028

Bertrand, S., Hughen, K., Sepúlveda, J., & Pantoja, S. (2014). Late Holocene covariability of the southern westerlies and sea surface temperature in northern Chilean Patagonia. *Quaternary Science Reviews*, *105*, 195–208. https://doi.org/10.1016/j.quascirev.2014.09.021

Blisniuk, P. M., Stern, L. A., Chamberlain, C. P., Zeitler, P. K., Ramos, V. A., Sobel, E. R., … Warkus, F. (2006). Links between mountain uplift, climate, and surface processes in the southern Patagonian Andes. *Frontiers in Earth Sciences*, *20*, 429–440. https://doi.org/10.1007/978-3-540-48684-8_20

Boulton, G. S., & Clark, C. D. (1990). The Laurentide ice sheet through the last glacial cycle: The topology of drift lineations as a key to the dynamic behaviour of former ice sheets. *Earth and Environmental Science Transactions of the Royal Society of Edinburgh*, *81*(4), 327–347. https://doi.org/10.1017/S0263593300020836

Briner, J. P., Miller, G. H., Davis, P. T., & Finkel, R. C. (2006). Cosmogenic radionuclides from fiord landscapes support differential erosion by overriding ice sheets. *Geological Society of America Bulletin*, *118*, 406–420. https://doi.org/10.1130/B25716.1

Briner, J. P., Miller, G. H., Finkel, R., & Hess, D. P. (2008). Glacial erosion at the fjord onset zone and implications for the organization of ice flow on Baffin Island, Arctic Canada. *Geomorphology*, *97*, 126–134. https://doi.org/10.1016/j.geomorph.2007.02.039

Cande, S. C., & Leslie, R. B. (1986). Late Cenozoic tectonics of the southern Chile trench. *Journal of Geophysical Research*, *91*, 471–496. https://doi.org/10.1029/JB091iB01p00471

Carel, M., Siani, G., & Delpech, G. (2011). Tephrostratigraphy of a deep-sea sediment sequence off the south Chilean margin: New insight into the Hudson volcanic activity since the last glacial period. *Journal of Volcanology and Geothermal Research*, *208*, 99–111. https://doi.org/10.1016/j.jvolgeores.2011.09.011

Catuneanu, O. (2006). *Principles of sequence stratigraphy*. Amsterdam, The Netherlands: Elsevier.

Cembrano, J., Lavenu, A., Reynolds, P., Arancibia, G., López, G., & Sanhueza, A. (2002). Late Cenozoic transpressional ductile deformation north of the Nazca-South America–Antarctica triple junction. *Tectonophysics*, *354*, 289–314. https://doi.org/10.1016/S0040-1951(02)00388-8

Champagnac, J. D., Molnar, P., Sue, C., & Herman, F. (2012). Tectonics, climate, and mountain topography. *Journal of Geology*, *117*, https://doi.org/10.1029/2011JB008348

Champagnac, J. D., Valla, P. G., & Herman, F. (2014). Late-Cenozoic relief evolution under evolving climate: A review. *Tectonophysics*, *614*, 44–65. https://doi.org/10.1016/j.tecto.2013.11.037

Christeleit, E. C., Brandon, M. T., & Shuster, D. L. (2017). Miocene development of alpine glacial relief in the Patagonian Andes, as revealed by low-temperature thermochronometry. *Earth and Planetary Science Letters*, *460*, 152–163. https://doi.org/10.1016/j.epsl.2016.12.019

DaSilva, J. L., Anderson, J. B., & Stravers, J. (1997). Seismic facies changes along a nearly continuous 24 latitudinal transect: The fjords of Chile and the northern Antarctic Peninsula. *Marine Geology*, *143*, 103–123. https://doi.org/10.1016/S0025-3227(97)00092-3

Diemer, J. A., & Forsythe, R. (1995). Grain size variations within slope facies recovered from the Chile Margin Triple Junction. In S. D. Lewis, J. H. Behrmann, R. J. Musgrave, & S. C. Cande (Eds.), *Proceedings of ODP scientific results* (Vol. *141*, pp. 79–94). College Station, TX: Ocean Drilling Program.

Dietrich, R., Ivins, E. R., Casassa, G., Lange, H., Wendt, J., & Fritsche, M. (2010). Rapid crustal uplift in Patagonia due to enhanced ice loss. *Earth and Planetary Science Letters*, *289*, 22–29. https://doi.org/10.1016/j.epsl.2009.10.021

D'Orazio, M., Innocenti, F., Manetti, P., Tamponi, M., Tonarini, S., González-Ferrán, O., … Omarini, R. (2003). The Quaternary calc-alkaline volcanism of the Patagonian Andes close to the Chile triple junction: Geochemistry and petrogenesis of volcanic rocks from the Cay and Maca volcanoes (∼45°S, Chile). *Journal of South American Earth Sciences*, *16*, 219–242. https://doi.org/10.1016/S0895-9811(03)00063-4

Egholm, D. L., Nielsen, S. B., Pedersen, V. K., & Lesemann, J. E. (2009). Glacial effects limiting mountain height. *Nature*, *460*, 884–887. https://doi.org/10.1038/nature08263

Encinas, A., Folguera, A., Oliveros, V., De Girolamo Del Mauro, L., Tapia, F., Riffo, R., … Álvarez, O. (2016). Late Oligocene–Early Miocene submarine volcanism and deep-marine sedimentation in an extensional basin of southern Chile: Implications for the tectonic development of the North Patagonian Andes. *Geological Society of America Bulletin*, *128*, 807–823. https://doi.org/10.1130/B31303.1

Fernandez, R. A., Anderson, J. B., Wellner, J. S., Minzoni, R. L., Hallet, B., & Smith, R. T. (2016). Latitudinal variation in glacial erosion rates from Patagonia and the Antarctic Peninsula (46°S−65°S). *Geological Society of America Bulletin*, *128*, 1000–1023. https://doi.org/10.1130/B31321.1

Garreaud, R., Lopez, P., Minvielle, M., & Rojas, M. (2013). Large-Scale Control on the Patagonian Climate. *Journal of Climate*, *26*, 215–230. https://doi.org/10.1175/JCLI-D-12-00001.1

Garzanti, E., Andò, S., & Vezzoli, G. (2009). Grain-size dependence of sediment composition and environmental bias in provenance studies. *Earth and Planetary Science Letters*, *277*, 422–432. https://doi.org/10.1016/j.epsl.2008.11.007

Garzanti, E., & Vezzoli, G. (2003). A classification of metamorphic grains in sands based on their composition and grade. *Journal of Sedimentary Research*, *73*, 830–837. https://doi.org/10.1306/012203730830

Glasser, N. F., & Ghiglione, M. C. (2009). Structural, tectonic and glaciological controls on the evolution of fjord landscapes. *Geomorphology*, *105*, 291–302. https://doi.org/10.1016/j.geomorph.2008.10.007

Glasser, N. F., & Jansson, K. N. (2005). Fast-flowing outlet glaciers of the Last Glacial Maximum Patagonian Icefield. *Quaternary Research*, *63*, 206–211. https://doi.org/10.1016/j.yqres.2004.11.002

Glasser, N. F., Jansson, K. N., Harrison, S., & Kleman, J. (2008). The glacial geomorphology and Pleistocene history of South America between 38°S and 56°S. *Quaternary Science Reviews*, *27*, 365–390. https://doi.org/10.1016/j.quascirev.2007.11.011

Gulick, S. P. S., Jaeger, J. M., Mix, A. C., Asahi, H., Bahlburg, H., Belanger, C. L., … Swartz, J. M. (2015). Mid-Pleistocene climate transition drives net mass loss from rapidly uplifting St. Elias Mountains, Alaska. *Proceedings of the National Academy of Sciences of the United States of America*, *112*, 15042–15047. https://doi.org/10.1073/pnas.1512549112

Heberer, B., Behrmann, J. H., & Rahn, M. K. (2011). Source-to-sink relationships along the South-Central Chilean margin: Evidence from detrital apatite fission-track analysis. *Basin Research*, *23*, 551–570. https://doi.org/10.1111/j.1365-2117.2011.00504.x

Heberer, B., Roser, G., Behrmann, J. H., Rahn, M., & Kopf, A. (2010). Holocene sediments from the Southern Chile Trench: A record of active margin magmatism, tectonics and palaeoseismicity. *Journal of the Geological Society*, *167*, 539–553. https://doi.org/10.1144/0016-76492009-015

Hein, A. S., Cogez, A., Darvill, C. M., Mendelova, M., Kaplan, M. R., Herman, F., … Rodés, Á. (2017). Regional mid-Pleistocene glaciation in central Patagonia. *Quaternary Science Reviews*, *164*, 77–94. https://doi.org/10.1016/j.quascirev.2017.03.023

Herman, F., & Brandon, M. (2015). Mid-latitude glacial erosion hotspot related to equatorial shifts in southern Westerlies. *Geology*, *43*, 987–990. https://doi.org/10.1130/G37008.1

Herman, F., Seward, D., Valla, P. G., Carter, A., Kohn, B., Willett, S. D., & Ehlers, T. A. (2013). Worldwide acceleration of mountain erosion under a cooling climate. *Nature*, *504*, 423–426. https://doi.org/10.1038/nature12877

Hervé, F., Fanning, C. M., & Pankhurst, R. J. (2003). Detrital zircon age patterns and provenance of the metamorphic complexes of southern Chile. *Journal of South American Earth Sciences*, *16*, 107–123. https://doi.org/10.1016/S0895-9811(03)00022-1

Hervé, F., Mpodozis, C., Davidson, J. P., & Godoy, E. (1981). Observaciones estructurales y petrográficas en el basamenro metamorfico del archiìelago de Los Chonos, entre el Canal King y el Canal Ninualac, Aysen. *Andean Geology*, 3–16.

Ho, S. L., Mollenhauer, G., Lamy, F., Martínez-Garcia, A., Mohtadi, M., Gersonde, R., … Tiedemann, R. (2012). Sea surface temperature variability in the Pacific sector of the Southern Ocean over the past 700 kyr. *Paleoceanography*, *27*, 380–416. https://doi.org/10.1029/2012PA002317

Hubbard, A., Hein, A. S., Kaplan, M. R., Hulton, N. R. J., & Glasser, N. (2005). A modelling reconstruction of the Last Glacial Maximum ice sheert and its deglaciation in the vicinity of the northern Patagonian Icefield, South America. *Geografiska Annaler: Series A, Physical Geography*, *87*, 375–391. https://doi.org/10.1111/j.0435-3676.2005.00264.x

Hulton, N., Purves, R. S., McCulloch, R. D., Sugden, D. E., & Bentley, M. J. (2002). The last glacial maximum and deglaciation in southern South America. *Quaternary Science Reviews*, *21*, 233–241. https://doi.org/10.1016/S0277-3791(01)00103-2

Ingersoll, R. V., Bullard, T. F., Ford, R. L., Grimm, J. P., Pickle, J. D., & Sares, S. W. (1984). The effect of grain size on detrital modes: A test of the Gazzi-Dickinson point-counting method. *Journal of Sedimentary Research*, *54*, 103–116. https://doi.org/10.1306/212F83B9-2B24-11D7-8648000102C1865D

Jacobsen, S. B., & Wasserburg, G. J. (1980). Sm-Nd isotopic evolution of chondrites. *Earth and Planetary Science Letters*, *50*(1), 139–155. https://doi.org/10.1016/0012-821X(80)90125-9

Jaeger, J. M., & Koppes, M. N. (2016). The role of the cryosphere in source-to-sink systems. *Earth-Science Reviews*, *153*, 43–76. https://doi.org/10.1016/j.earscirev.2015.09.011

Jamieson, S. S. R., Sugden, D. E., & Hulton, N. R. J. (2010). The evolution of the subglacial landscape of Antarctica. *Earth and Planetary Science Letters*, *293*, 1–27. https://doi.org/10.1016/j.epsl.2010.02.012

Jouzel, J., Masson-Delmotte, V., Cattani, O., Dreyfus, G., Falourd, S., Hoffmann, G., … Wolff, E. W. (2007). Orbital and millennial Antarctic climate variability over the past 800,000 years. *Science*, *317*, 793–796. https://doi.org/10.1126/science.1141038

Kamenov, G. D., Perfit, M. R., Mueller, P. A., & Jonasson, I. R. (2008). Controls on magmatism in an island arc environment: Study of lavas and sub-arc xenoliths from the Tabar-Lihir-Tanga-Feni island chain, Papua New Guinea. *Contributions to Mineralogy and Petrology*, *155*, 635–656. https://doi.org/10.1007/s00410-007-0262-0

Kaplan, M. R., Douglass, D. C., Singer, B. S., Ackert, R. P., & Caffee, M. W. (2005). Cosmogenic nuclide chronology of pre-last glacial maximum moraines at Lago Buenos Aires, 46°S, Argentina. *Quaternary Research*, *63*, 301–315.

Kaplan, M. R., Hein, A. S., Hubbard, A., & Lax, S. M. (2009). Can glacial erosion limit the extent of glaciation? *Geomorphology*, *103*, 172–179. https://doi.org/10.1016/j.geomorph.2008.04.020

Kilian, R., & Behrmann, J. H. (2003). Geochemical constraints on the sources of Southern Chile Trench sediments and their recycling in arc magmas of the Southern Andes. *Journal of the Geological Society*, *160*, 57–70. https://doi.org/10.1144/0016-764901-143

Lamy, F., Hebbeln, D., & Wefer, G. (1999). High-resolution marine record of climatic change in mid-latitude Chile during the last 28,000 years based on terrigenous sediment parameters. *Quaternary Research*, *51*, 83–93. https://doi.org/10.1006/qres.1998.2010

Lamy, F., Kilian, R., Arz, H. W., Francois, J.-P., Kaiser, J., Prange, M., & Steinke, T. (2010). Holocene changes in the position and intensity

of the southern westerly wind belt. *Nature Geoscience*, *3*, 695–699. https://doi.org/10.1038/ngeo959

Lange, D., Cembrano, J., Rietbrock, A., Haberland, C., Dahm, T., & Bataille, K. (2008). First seismic record for intra-arc strike-slip tectonics along the Liquiñe-Ofqui fault zone at the obliquely convergent plate margin of the southern Andes. *Tectonophysics*, *455*, 14–24. https://doi.org/10.1016/j.tecto.2008.04.014

Lisiecki, L. E., & Raymo, M. E. (2005). A Pliocene-Pleistocene stack of 57 globally distributed benthic δ18O records. *Paleoceanography*, *20*(1), https://doi.org/10.1029/2004PA001071

Lopez-Escobar, L., Kilian, R., Kempton, P. D., & Tagiri, M. (1993). Petrography and geochemistry of Quaternary rocks from the Southern Volcanic Zone of the Andes between 41 30'and 46 00'S, Chile. *Andean Geology*, *20*, 33–55.

Lougheed, B. C., & Obrochta, S. P. (2016). MatCal: Open source Bayesian 14C age calibration in MatLab. *Journal of Open Research Software*, *4*(1), e42. https://doi.org/10.5334/jors.130

Marsaglia, K. M., & Tazaki, K. (1992). Diagenetic trends in ODP Leg 126 sandstone. In F. Kantaro, Y. Matsuo, A. Nishimura, M. Koyama, & K. S. Rodolfo (Eds.), *Proceedings of the ocean drilling program, scientific results* (Vol. *126*, pp. 125–138). College Station, TX: Ocean Drilling Program.

Marsaglia, K. M., Torrez, X. V., Padilla, I., & Rimkus, K. C. (1995). Provenance of Pleistocene and Pliocene sand and sandstone, ODP Leg 141, Chile Margin. In S. D. Lewis, J. H. Behrmann, R. J. Musgrave, & S. C. Cande (Eds.), *Proceedings of ODP scientific results* (Vol. *141*, pp. 133–151). College Station, TX: Ocean Drilling Program.

Mercer, J. H., & Sutter, J. F. (1982). Late Miocene-Earliest Pliocene glaciation in southern Argentina: Implications for global ice-sheet. *Palaeogeography, Palaeoclimatology, Palaeoecology*, *38*, 185–206.

Miller, K. G., Kominz, M. A., Browning, J. V., Wright, J. D., & Mountain, G. (2005). The Phanerozoic record of global sea-level change. *Science*, *310*, 1293–1298. https://doi.org/10.1126/science.1116412

Molnar, P., & England, P. (1990). Late Cenozoic uplift of mountain ranges and global climate change: Chicken or egg? *Nature*, *346*, 29–34. https://doi.org/10.1038/346029a0

Montade, V., Combourieu Nebout, N., Kissel, C., Haberle, S. G., Siani, G., & Michel, E. (2013). Vegetation and climate changes during the last 22,000 yr from a marine core near Taitao Peninsula, southern Chile. *Palaeogeography, Palaeoclimatology, Palaeoecology*, *369*, 335–348. https://doi.org/10.1016/j.palaeo.2012.11.001

Montelli, A., Dowdeswell, J. A., Ottesen, D., & Johansen, S. E. (2017). Ice-sheet dynamics through the Quaternary on the mid-Norwegian continental margin inferred from 3D seismic data. *Marine and Petroleum Geology*, *80*, 228–242. https://doi.org/10.1016/j.marpetgeo.2016.12.002

Montgomery, D. R., Balco, G., & Willett, S. D. (2001). Climate, tectonics, and the morphology of the Andes. *Geology*, *29*, 579–582. https://doi.org/10.1130/0091-7613(2001)029<0579:CTATMO>2.0.CO;2

Moreno, P. I., & León, A. L. (2003). Abrupt vegetation changes during the last glacial to Holocene transition in mid-latitude South America. *Journal of Quaternary Science*, *18*, 787–800. https://doi.org/10.1002/jqs.801

Naranjo, J. A., & Stern, C. R. (1998). Holocene explosive activity of Hudson Volcano, southern Andes. *Bulletin of Volcanology*, *59*(4), 291–306. https://doi.org/10.1007/s004450050193

Ó Cofaigh, C., Andrews, J. T., Jennings, A. E., Dowdeswell, J. A., Hogan, K. A., Kilfeather, A. A., & Sheldon, C. (2012). Glacimarine lithofacies, provenance and depositional processes on a West Greenland trough-mouth fan. *Journal of Quaternary Science*, *28*, 13–26. https://doi.org/10.1002/jqs.2569

Orihashi, Y., Naranjo, J. A., Motoki, A., Sumino, H., Hirata, D., Anma, R., & Nagao, K. (2004). Quaternary volcanic activity of Hudson and Lautaro volcanoes, Chilean Patagonia: New constraints from K-Ar ages. *Revista Geológica De Chile*, *31*, 1–19. https://doi.org/10.4067/S0716-02082004000200002

Pankhurst, R. J., Weaver, S. D., Hervé, F., & Larrondo, P. (1999). Mesozoic-Cenozoic evolution of the North Patagonian batholith in Aysen, southern Chile. *Journal of the Geological Society*, *156*, 673–694. https://doi.org/10.1144/gsjgs.156.4.0673

Pardo-Casas, F., & Molnar, P. (1987). Relative motion of the Nazca (Farallon) and South American Plates since late Cretaceous time. *Tectonics*, *6*, 233–248. https://doi.org/10.1029/TC006i003p00233

Powell, R. D., & Cooper, J. M. (2002). A glacial sequence stratigraphic model for temperate, glaciated continental shelves. *Geological Society, London, Special Publications*, *203*, 215–244. https://doi.org/10.1144/GSL.SP.2002.203.01.12

Rabassa, J., Coronato, A., & Martinez, O. (2011). Late Cenozoic glaciations in Patagonia and Tierra del Fuego: An updated review. *Biological Journal of the Linnean Society*, *103*, 316–335. https://doi.org/10.1111/j.1095-8312.2011.01681.x

Ramos, V. A., & Ghiglione, M. C. (2008). Tectonic evolution of the Patagonian Andes. *Developments in Quaternary Sciences*, *11*, 57–71.

Reimer, P. J., Bard, E., Bayliss, A., Beck, J. W., Blackwell, P. G., Ramsey, C. B., … van der Plicht, J. (2013). IntCal13 and Marine13 radiocarbon age calibration curves 0–50,000 years cal BP. *Radiocarbon*, *55*, 1869–1887. https://doi.org/10.2458/azu_js_rc.55.16947

Richard, P., Shimazu, N., & Allegre, C. J. (1976). ^{143}Nd/^{144}Nd, a natural tracer: An application to oceanic basalt. *Earth and Planetary Science Letters*, *31*, 269–278.

Rodrigo, C. (2008). Submarine topography in the Chilean North Patagonian channels. In N. Silva & S. Palma (Eds.), *Progress in the oceanographic knowledge of Chilean interior waters, from Puerto Montt to Cape Horn* (pp. 19–23). Valparaiso, Chile: Comité Oceanográfico Nacional - Pontificia Universidad Católica de Valparaíso.

Schönfeld, J., Spiegler, D., & Erlenkeuser, H. (1995). Late Quaternary stable isotope record of planktonic and benthic foraminifers: Site 861, Chile Triple Junction. In S. D. Lewis, J. H. Behrmann, R. J. Musgrave, & S. C. Cande (Eds.), *Proceedings of ODP scientific results* (Vol. *141*, pp. 235–240). College Station, TX: Ocean Drilling Program.

Sernageomin. (2003). Mapa Geológico de Chile: versión digital. Servicio Nacional de Geología y Minería, Publicación Geológica Digital, No. 4 (CD-ROM, versión1.0, 2003). Santiago.

Siani, G., Colin, C., Michel, E., Carel, M., Richter, T., Kissel, C., & Dewilde, F. (2010). Late Glacial to Holocene terrigenous sediment record in the Northern Patagonian margin: Paleoclimate implications. *Palaeogeography, Palaeoclimatology, Palaeoecology*, *297*, 26–36. https://doi.org/10.1016/j.palaeo.2010.07.011

Siani, G., Michel, E., De Pol-Hoz, R., DeVries, T., Lamy, F., Carel, M., … Lourantou, A. (2013). Carbon isotope records reveal precise timing of enhanced Southern Ocean upwelling during the last deglaciation. *Nature Communications*, *4*, 1–9. https://doi.org/10.1038/ncomms3758

Sievers, H., & Silva, N. (2008). Water masses and circulation in austral Chilean channels and fjords. In N. Silva & S. Palma (Eds.), *Progress*

in the oceanographic knowledge of Chilean interior waters, from Puerto Montt to Cape Horn (pp. 53–58). Valparaíso, Chile: Comité Oceanográfico Nacional – Pontificia Universidad Católica de Valparaíso.

Silva, N., & Guzmán, D. (2006). Condiciones oceanográficas, físicas y químicas, entre boca del Guafo y fiordo Aysén (Crucero Cimar 7 Fiordos). *Ciencia Y Tecnología Del Mar*, *29*, 25–44.

Singer, B. S., Ackert, R. P., & Guillou, H. (2004). ^{40}Ar/^{39}Ar and K-Ar chronology of Pleistocene glaciations in Patagonia. *Geological Society of America Bulletin*, *116*, 434–517. https://doi.org/10.1130/B25177.1

Stokes, C. R., Margold, M., Clark, C. D., & Tarasov, L. (2016). Ice stream activity scaled to ice sheet volume during Laurentide Ice Sheet deglaciation. *Nature*, *530*, 322–326. https://doi.org/10.1038/nature16947

Strand, K., Marsaglia, K., & Forsythe, R. (1995). Outer margin depositional systems near the Chile Margin Triple Junction. In S. D. Lewis, J. H. Behrmann, R. J. Musgrave, & S. C. Cande (Eds.), *Proceedings of ODP scientific results* (Vol. *141*, pp. 379–397). College Station, TX: Ocean Drilling Program.

Strub, P. T., James, C., Montecino, V., Rutllant, J. A., & Blanco, J. L. (2019). Ocean circulation along the southern Chile transition region (38°–46°S): Mean, seasonal and interannual variability, with a focus on 2014–2016. *Progress in Oceanography*, *172*, 159–198. https://doi.org/10.1016/j.pocean.2019.01.004

Strub, P. T., Mesias, J. M., Montecino, V., Rutllant, J., & Salinas, S. (1998). Coastal ocean circulation off western South America. *The Sea*, *11*, 273–313.

Suárez, M., De La Cruz, R., & Bell, C. M. (2000). Timing and origin of deformation along the Patagonian fold and thrust belt. *Geological Magazine*, *137*(4), 345–353. https://doi.org/10.1017/S0016756800004192

Thomson, S. N. (2002). Late Cenozoic geomorphic and tectonic evolution of the Patagonian Andes between latitudes 42˚S and 46˚S: An appraisal based on fission-track results from the transpressional intra-arc Liquiñe-Ofqui fault zone. *Geolological Society of America Bulletin*, *114*, 1159–1173.

Thomson, S. N., Brandon, M. T., Tomkin, J. H., Reiners, P. W., Vásquez, C., & Wilson, N. J. (2010). Glaciation as a destructive and constructive control on mountain building. *Nature*, *467*, 313–317. https://doi.org/10.1038/nature09365

Thomson, S. N., Hervé, F., & Stöckhert, B. (2001). Mesozoic-Cenozoic denudation history of the Patagonian Andes (southern Chile) and its correlation to different subduction processes. *Tectonics*, *20*, 693–711. https://doi.org/10.1029/2001TC900013

Thornburg, T. M., & Kulm, L. D. (1987). Sedimentation in the Chile Trench; petrofacies and provenance. *Journal of Sedimentary Research*, *57*, 55–74. https://doi.org/10.1306/212F8AA3-2B24-11D7-8648000102C1865D

Tsuchiya, M., & Talley, L. D. (1998). A Pacific hydrographic section at 88°W: Water-property distribution. *Journal of Geophysical Research*, *12*, 899–918. https://doi.org/10.1029/97JC03415

Tzedakis, P. C., Raynaud, D., McManus, J. F., Berger, A., Brovkin, V., & Kiefer, T. (2009). Interglacial diversity. *Nature Geoscience*, *2*, 751–755. https://doi.org/10.1038/ngeo660

VanLaningham, S., Pisias, N. G., Duncan, R. A., & Clift, P. D. (2009). Glacial–interglacial sediment transport to the Meiji Drift, northwest Pacific Ocean: Evidence for timing of Beringian outwashing. *Earth and Planetary Science Letters*, *277*, 64–72. https://doi.org/10.1016/j.epsl.2008.09.033

Villaseñor, T., Jaeger, J. M., & Foster, D. A. (2016). Linking Late Pleistocene alpine glacial erosion and continental margin sedimentation: Insights from ^{40}Ar/^{39}Ar dating of silt-sized sediment, Canterbury Basin, New Zealand. *Earth and Planetary Science Letters*, *433*, 303–316. https://doi.org/10.1016/j.epsl.2015.11.008

Völker, D., Geersen, J., Contreras-Reyes, E., & Reichert, C. (2013). Sedimentary fill of the Chile Trench (32–46°S): Volumetric distribution and causal factors. *Journal of the Geological Society*, *170*, 723–736. https://doi.org/10.1144/jgs2012-119

Weaver, S. G., Bruce, R., Nelson, E. P., Brueckner, H. K., & LeHuray, A. P. (1990). The Patagonian batholith at 48°S latitude, Chile; Geochemical and isotopic variations. *Geological Society of America Special Paper*, *241*, 33–50.

Willner, A. P., Hervé, F., & Massonne, H.-J. (2000). Mineral chemistry and pressure-temperature evolution of two contrasting high-pressure–low-temperature belts in the Chonos Archipelago, Southern Chile. *Journal of Petrology*, *41*, 309–330. https://doi.org/10.1093/petrology/41.3.309

Yanites, B. J., & Ehlers, T. A. (2012). Earth and planetary science letters. *Earth and Planetary Science Letters*, *325–326*, 63–75. https://doi.org/10.1016/j.epsl.2012.01.030

SUPPORTING INFORMATION

Additional supporting information may be found online in the Supporting Information section at the end of the article.

How to cite this article: Villaseñor T, Tentori D, Marsaglia KM, Pinto L. The changing Patagonian landscape: Erosion and westward sediment transfer paths in northern Patagonia during the Middle and Late Pleistocene. *Basin Res*. 2020;32:1035–1053. https://doi.org/10.1111/bre.12413